Adaptive Optics in Astronomy

- Real time compensation for atmospheric turbulence
- Restoring near-diffraction-limited performance at infrared wavelengths
- Now pushing image improvements to shorter wavelengths, larger fields, better and more stable image quality
- For detailed tutorials see.
  Claire Max: https://www.ucolick.org/~max/289/

Adaptive Optics - removing the effects of the atmosphere

A beam-splitter is used to separate the optical and IR light.
Infrared light is passed to the instrument via a deformable mirror – the science channel
While visible light is passed to a wavefront sensor where the tilts in subapertures of the wavefront are calculated
Error signals from these measurements are calculated and used to shape the deformable mirror
The control loop operates at about 100Hz

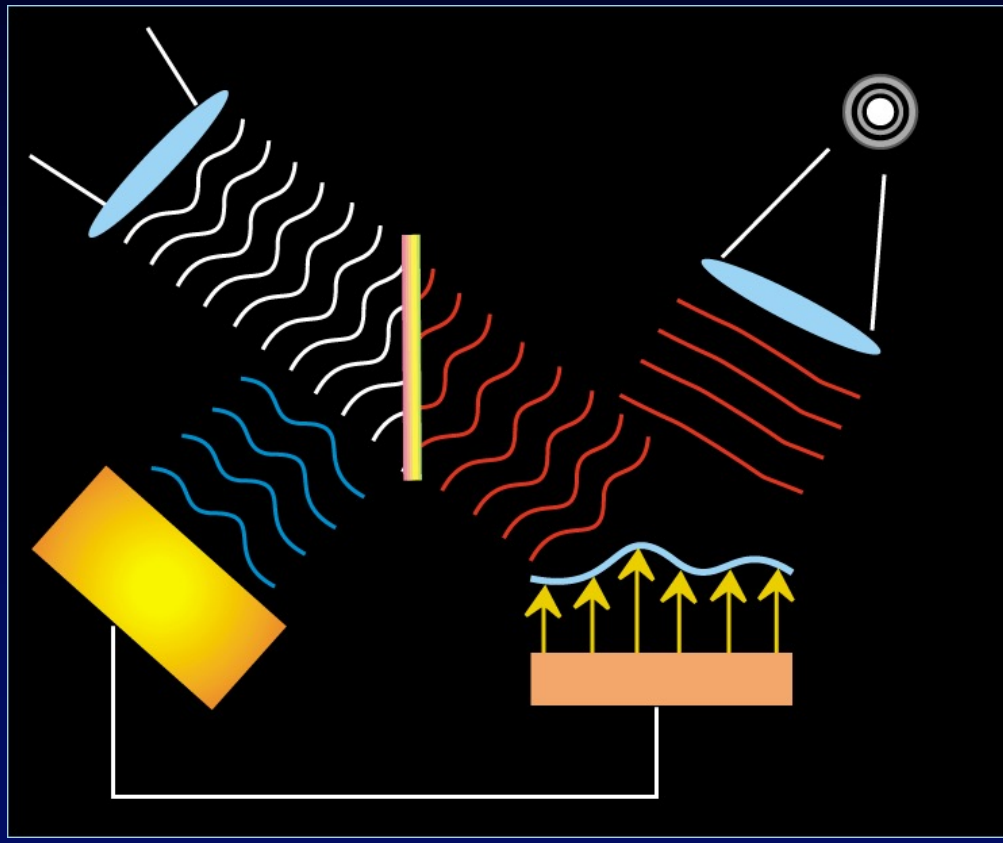

Adaptive Optics - removing the effects of the atmosphere

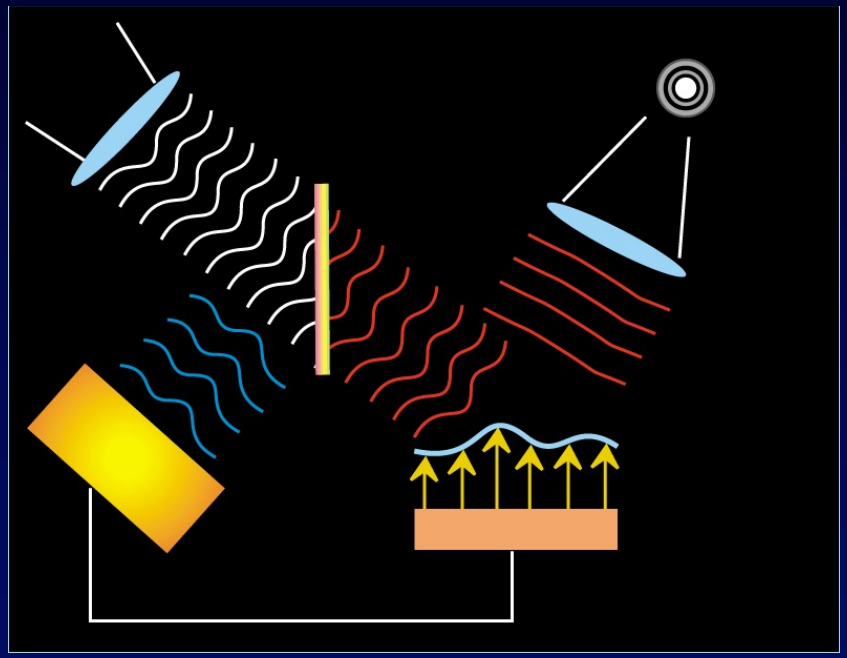

AO – real time computing and control challenges

- A number of different techniques are used for wavefront sensing, but the simplest conceptually is the Shack-Hartmann sensor
- The pupil is divided into a number of sub-apertures, typically each on the scale of r_0
- the tilt within each subaperture is determined by measuring the centroid of the sub-image – the displacement relative to the unaberrated pupil gives the tilt angle. A global reconstructor then estimates the overall shape
- A signal is applied to the matching actuators in the deformable mirror to counteract the tilt.
- This has to be done before the distortions change significantly

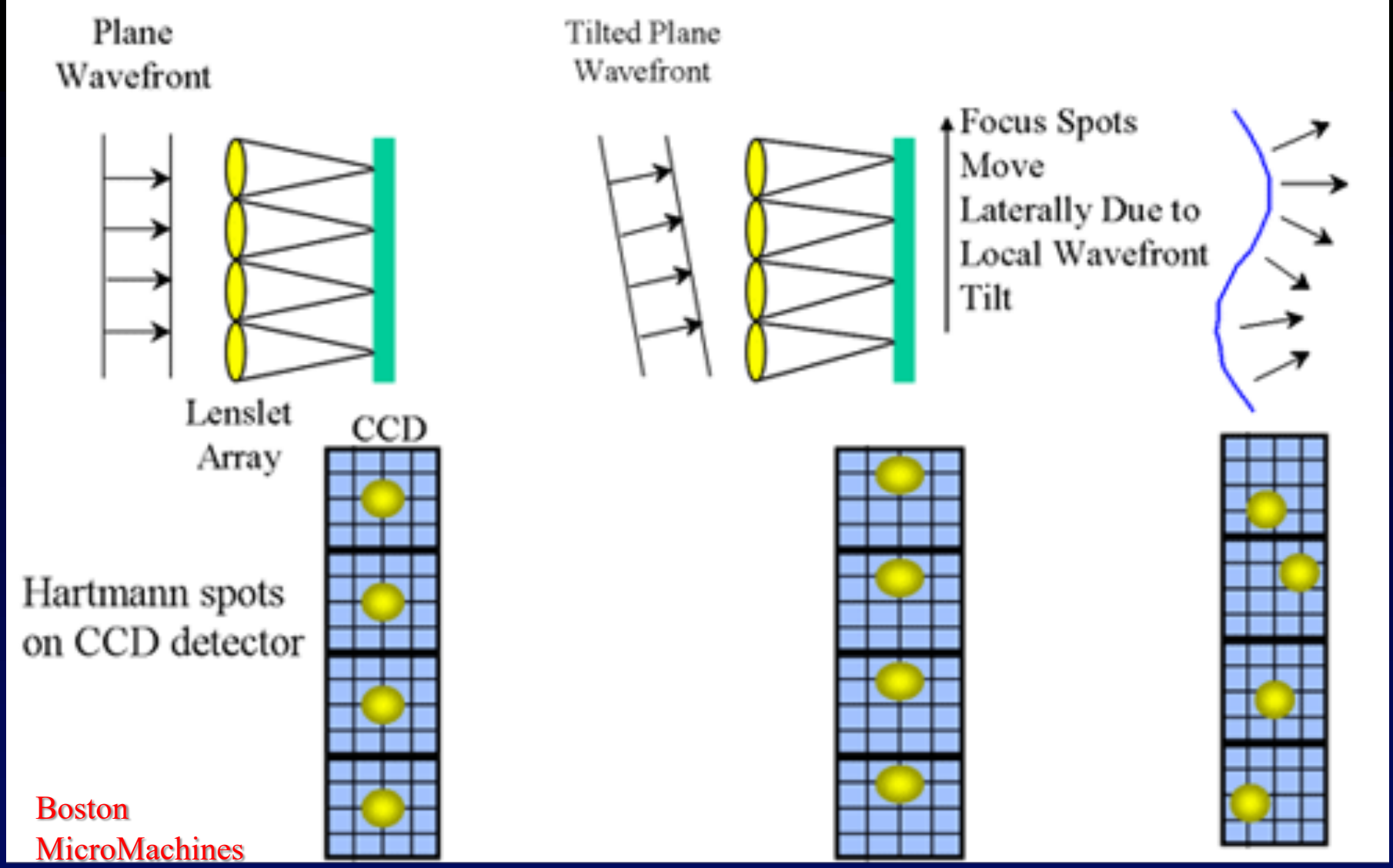

- Shack Hartmann WFS: For a large telescope, need 10s of subapertures across the pupil diameter and so the stellar flux from a guide star is divided into 100s or thousands of sub-apertures

Practical Considerations

r_0 the turbulence coherence length, or Fried Parameter, is the typical size of turbulent cells in the atmosphere. Typically 5cm to 20cm in the visible at good sites

Angular isoplanatism – the angular measure over which a compensated wavefront can be considered planar ($<\pi$ radians). At visible wavelengths the isoplanatic angle is about 2 arc seconds increasing to 10 arc seconds in the near infrared.

- Compensation in visible wavelengths (0.5um) requires a guide star of magnitude 10 or brighter.
- Compensation in infrared wavelengths (2.2um) allows guide stars down to magnitude 14.
- Small isoplanatic region around the guide star limits targets
  - Visible – 1/100,000 of the sky
  - IR – 1/1000 of the sky

Strehl

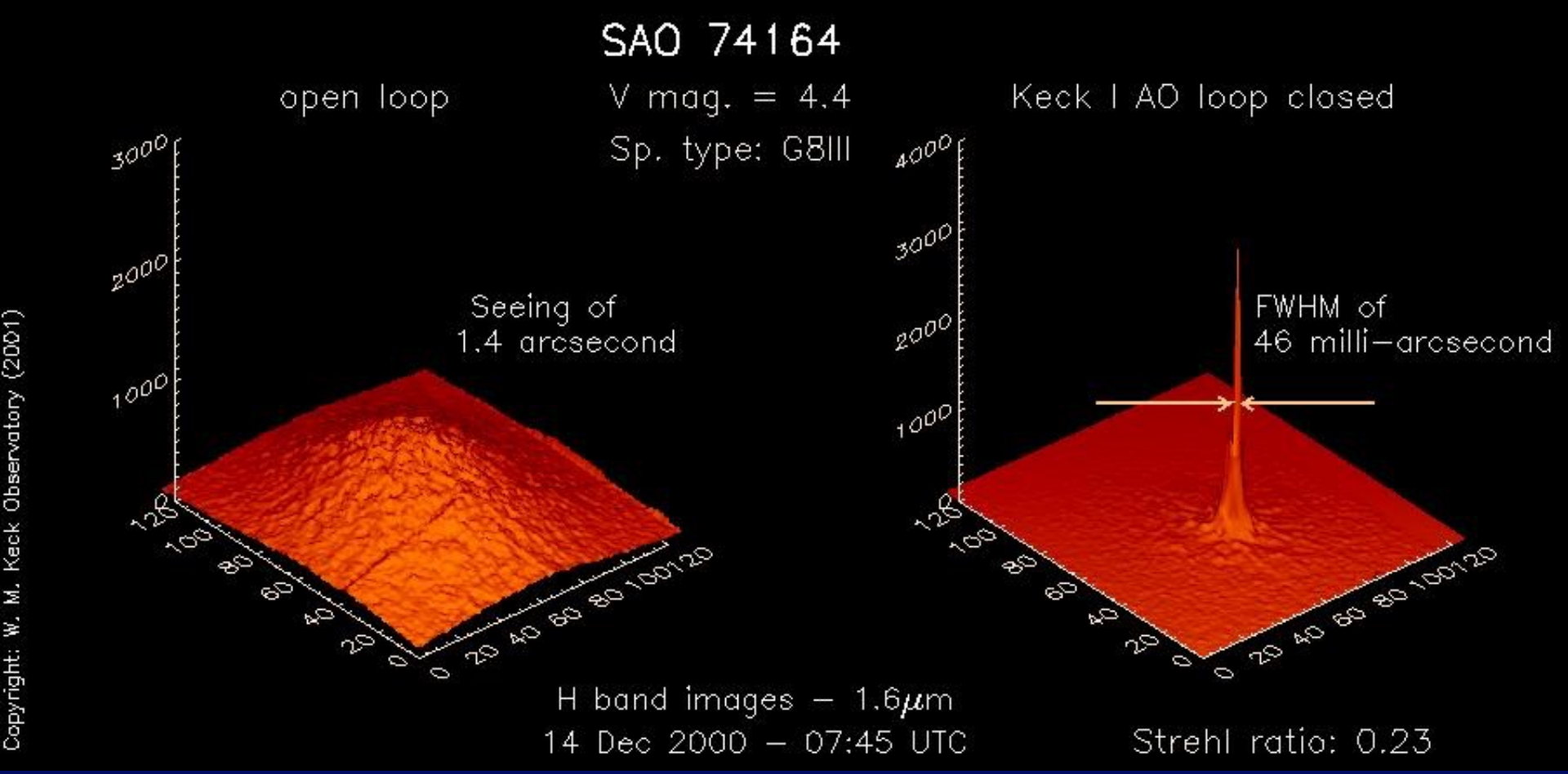

A measure of the quality of correction is the Strehl ratio – the fraction of intensity contained in the central maximum compared to the theoretical diffraction pattern

Isoplanatic Angle

Where a target is separated from a guide star by a significant angle, the column of turbulence along the path to the two objects diverges and leads to decorrelation.

AO correction falls off rapidly as the separation increases

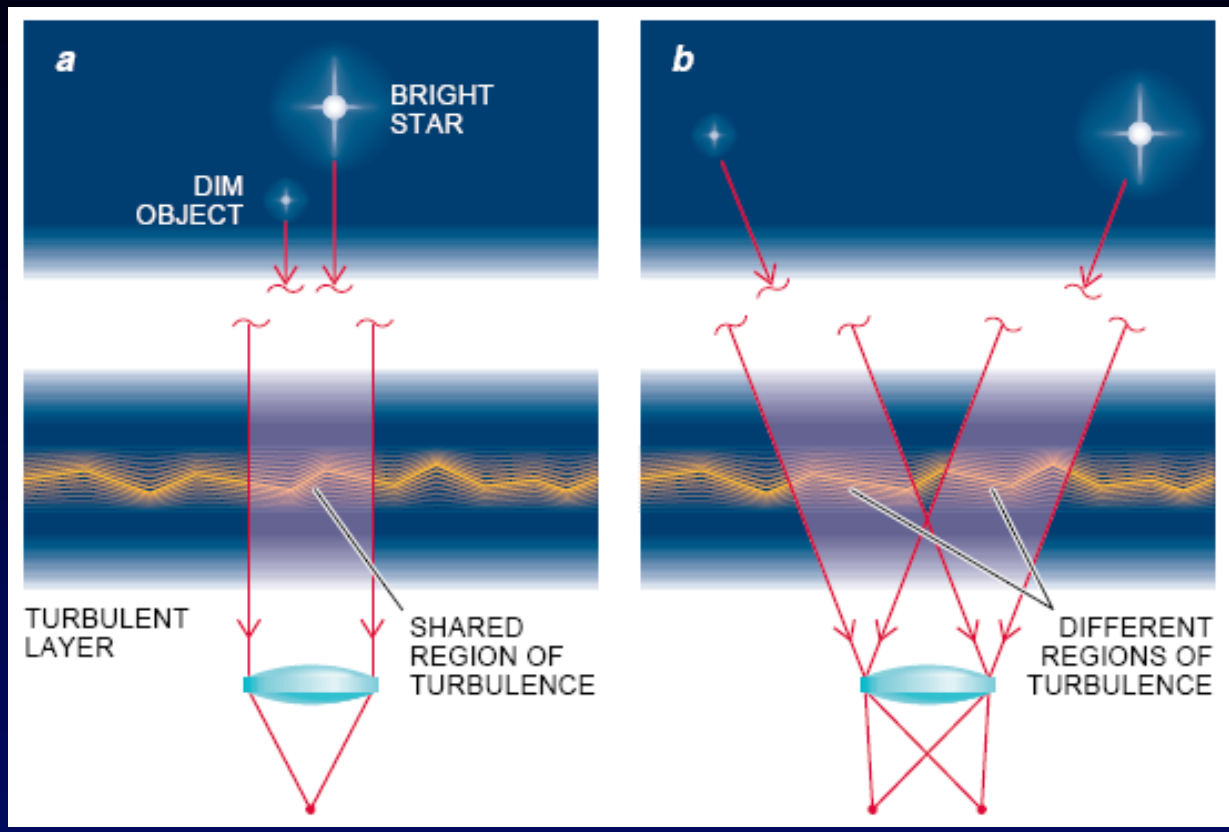

The definition of the atmospheric isoplanatic angle θ_0 is

$$\theta_0 = 0.31 \; r_0 / \; h$$

where h is the characteristic altitude of turbulence

WFS Sensitivity Limits

With frame rates ~1kHz, and e.g. 20 x 20 subapertures, the photon flux/ sample/subaperture is ~10^6 times lower than the photon flux/sec gathered by the telescope.

The light from each sub-aperture is imaged onto a small number of pixels and needs sufficient signal for the centroid to be measured.

The measurement error depends on the number of detected photons and α 1/SNR so there is a trade off between star brightness and quality of correction

With low-noise detectors, typically require stars of magnitude < 14 as AO guide stars for IR imaging

Laser Guide Stars

- The limited sky coverage can be improved by using ‘artificial stars’
- Generated with a 589nm sodium laser 90km above the telescope
- ~0.4 m launch telescope mounted behind the secondary or mounted on the top-end ring, with beam-forming and steering optics etc. Produces ~2arcsec ‘star’ at zenith, which is elongated at higher airmass due to Na layer thickness
- Laser star allows high order correction over most of the sky

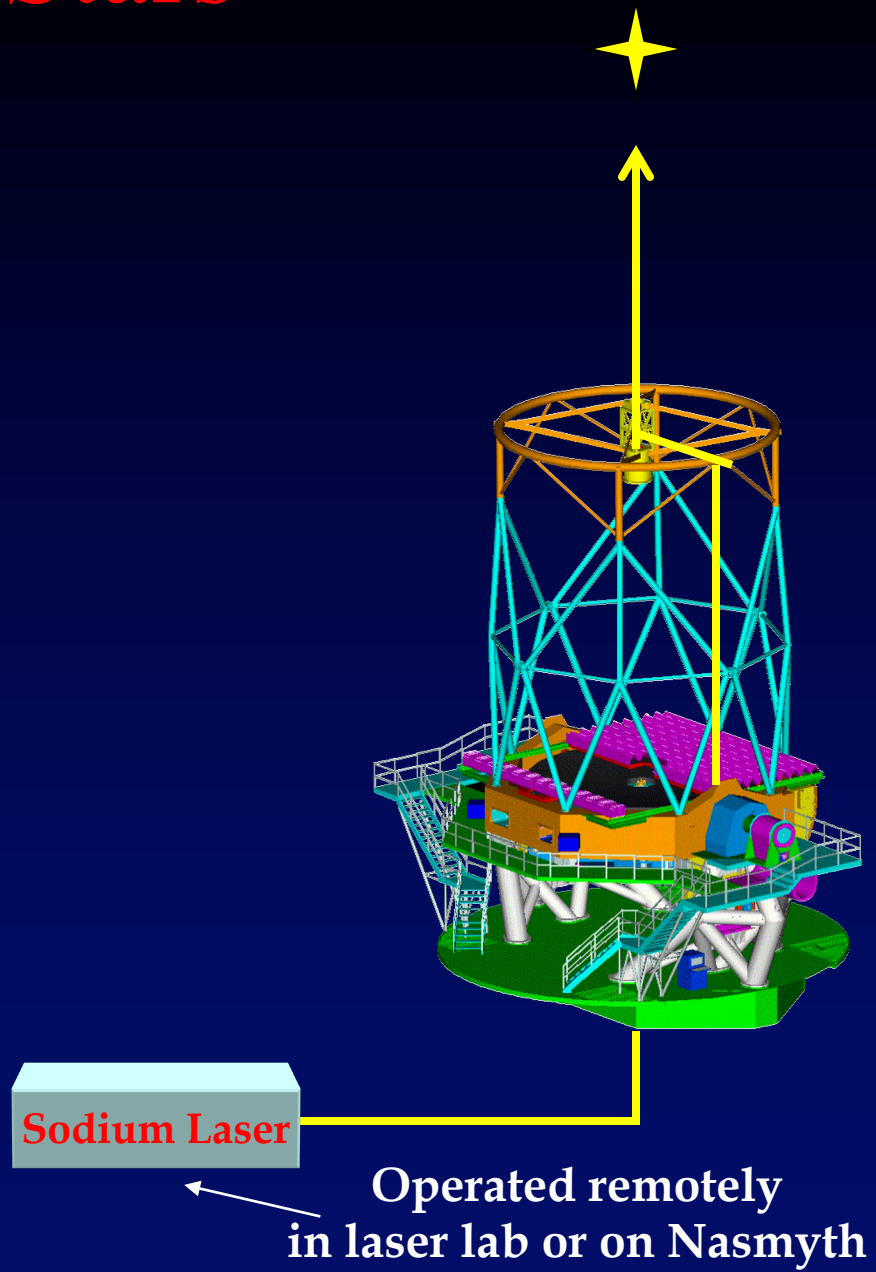

Limitations of Laser Stars

The laser beam passes through the atmosphere up to the sodium layer and the tilt component causes the position of the star to wander.
A natural guide star is used as the tilt component reference

The cone of light from the LGS samples a subset of the cylinder that the telescope beam encompasses so it does not cover some turbulence :focal anisoplatism or the Cone effect

Note that beam divergence is greater for smaller telescopes – ELTs win!

The distance to the sodium layer increases with zenith distance, so continuous refocussing or path length compensation is required

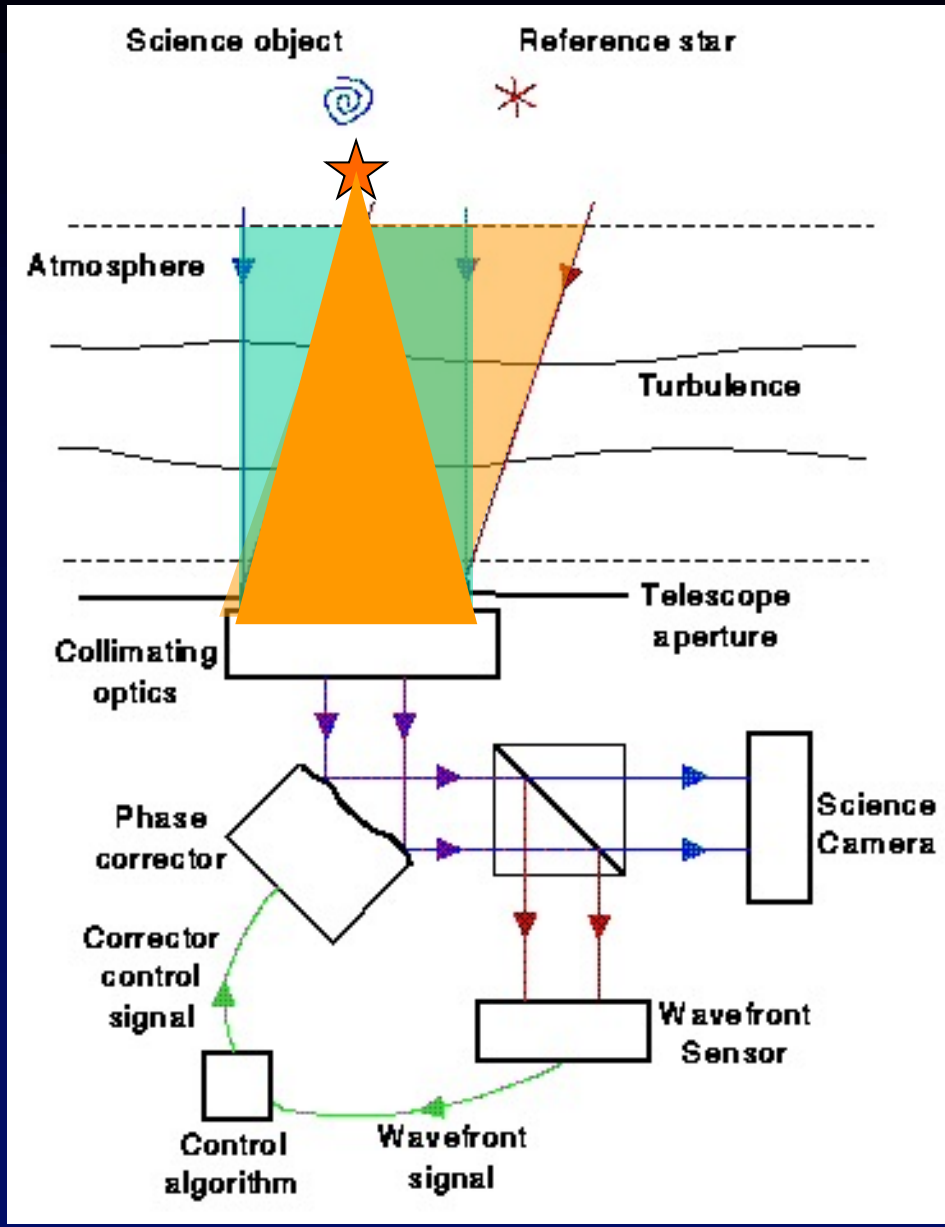

Advanced AO

- 4 (or more) LGS in a constellation can cover the full cylinder and give improved correction
- Combined with multiple deformable mirrors (DMs), conjugated to different altitudes, this gives complete sampling and improved correction for the atmosphere.
- Multi-conjugate AO - e.g GEMS at Gemini-S
- Xtreme AO with high density actuators to give very high strehl images – e.g for exoplanet searches

Tomography

1. Cone effect

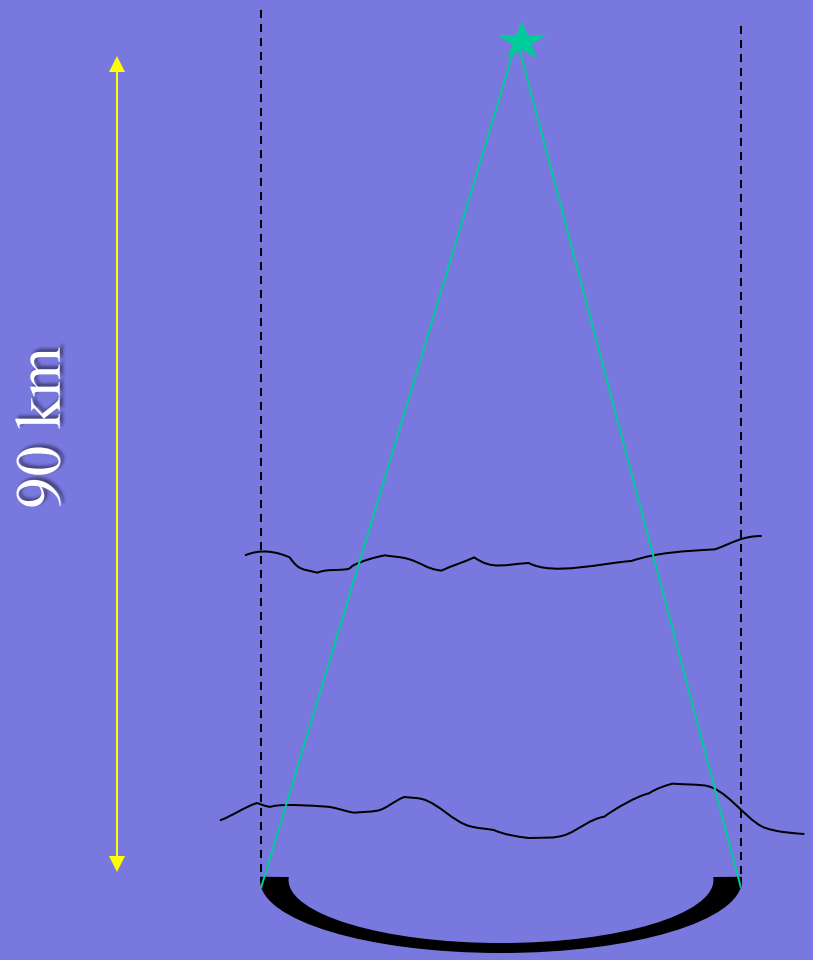

Tomography ?

2. Multiple guide star and tomography

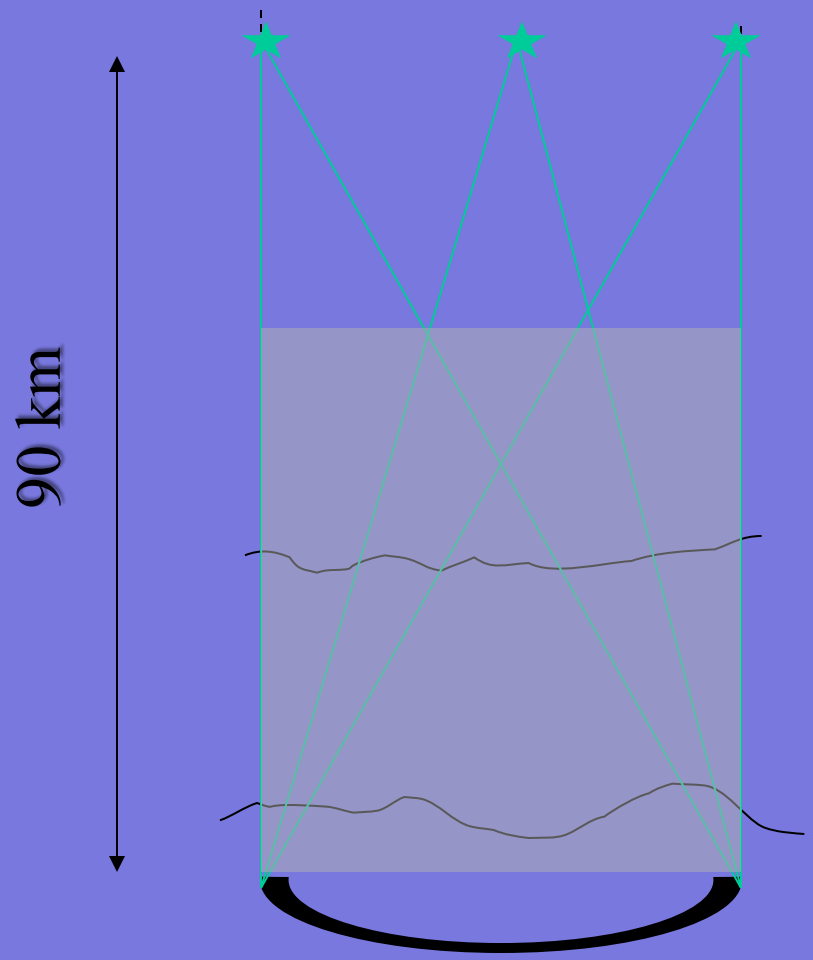

Multiconjugate

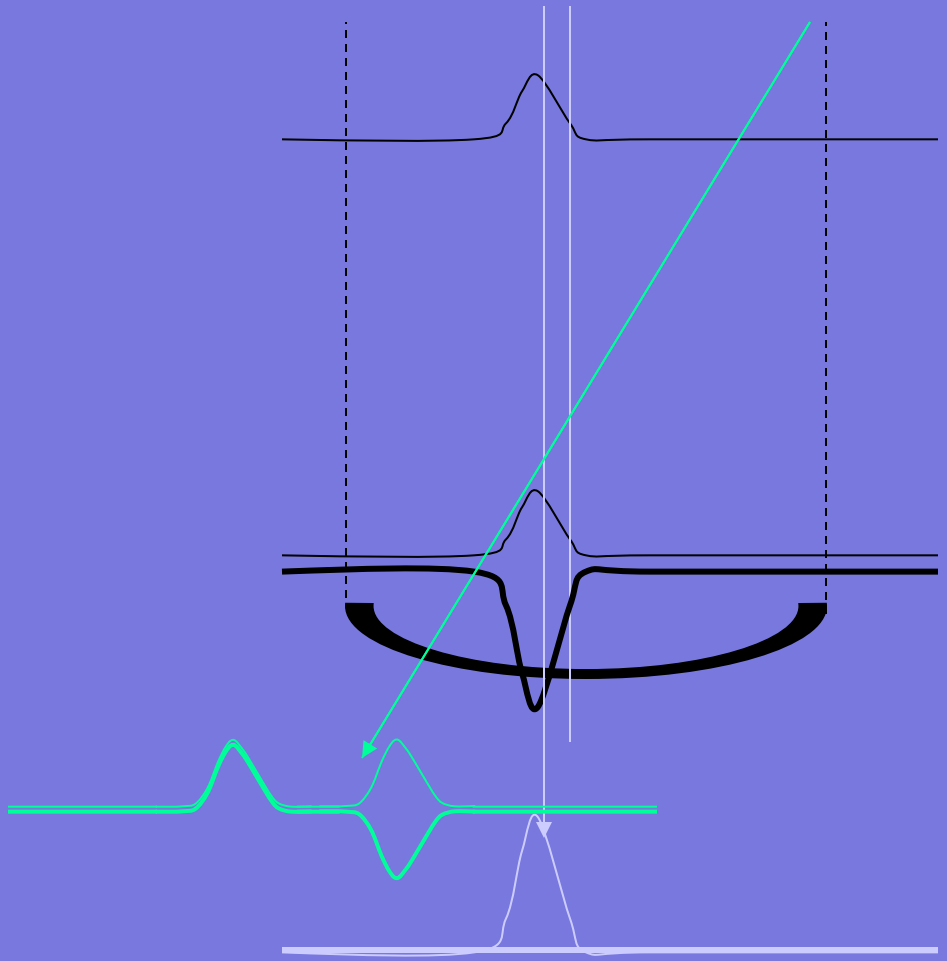

What is multiconjugate?

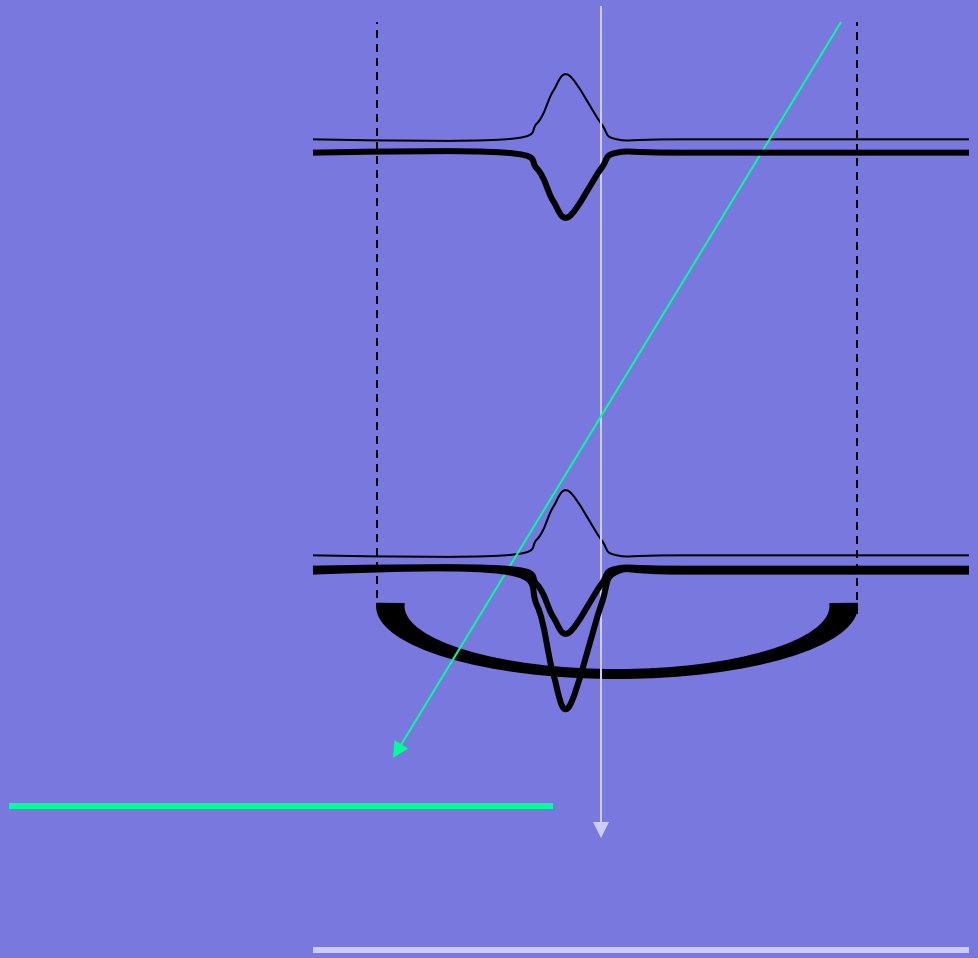

Multiconjugate AO

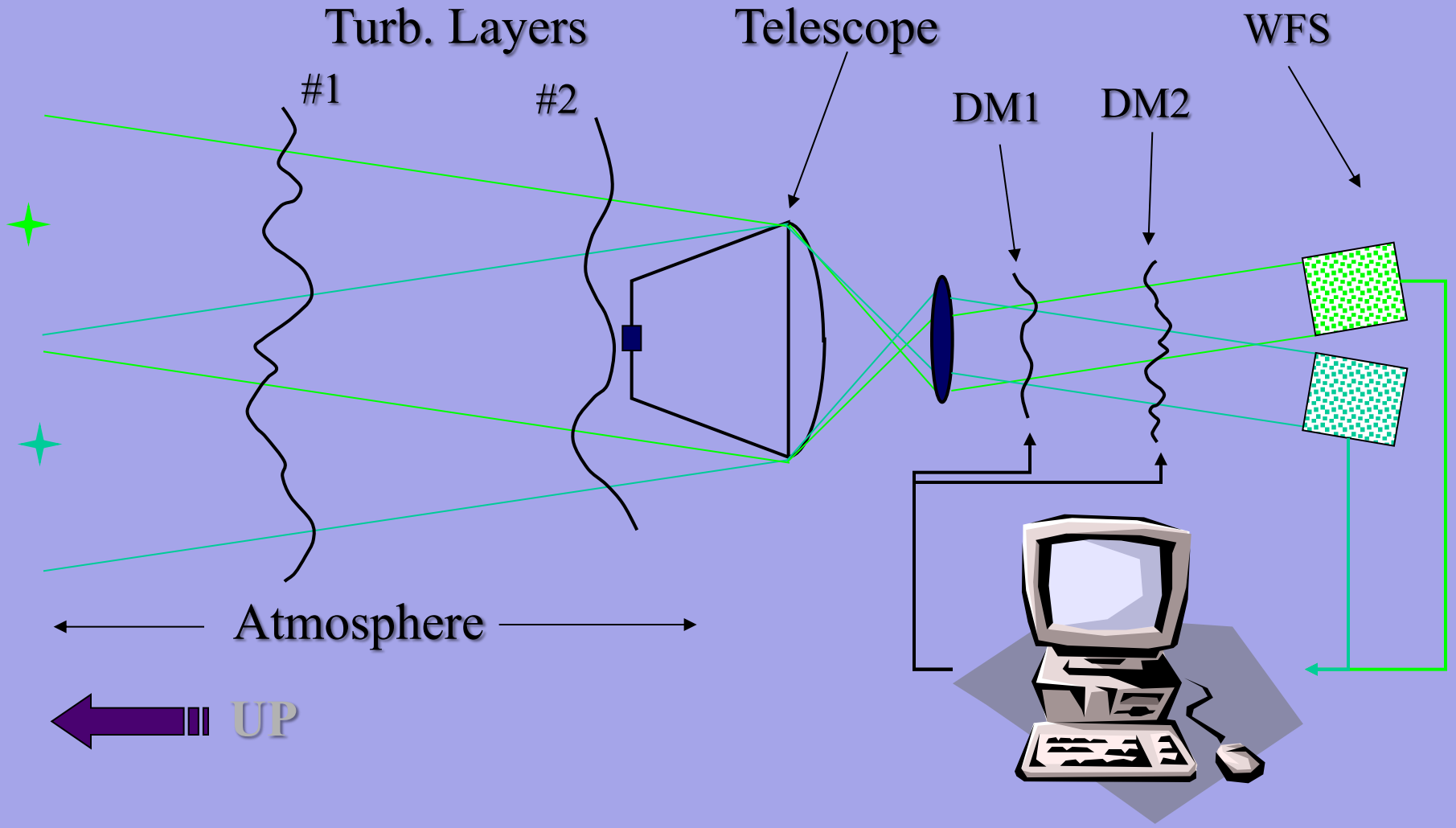

MCAO Performance Summary

Early NGS results, MK Profile

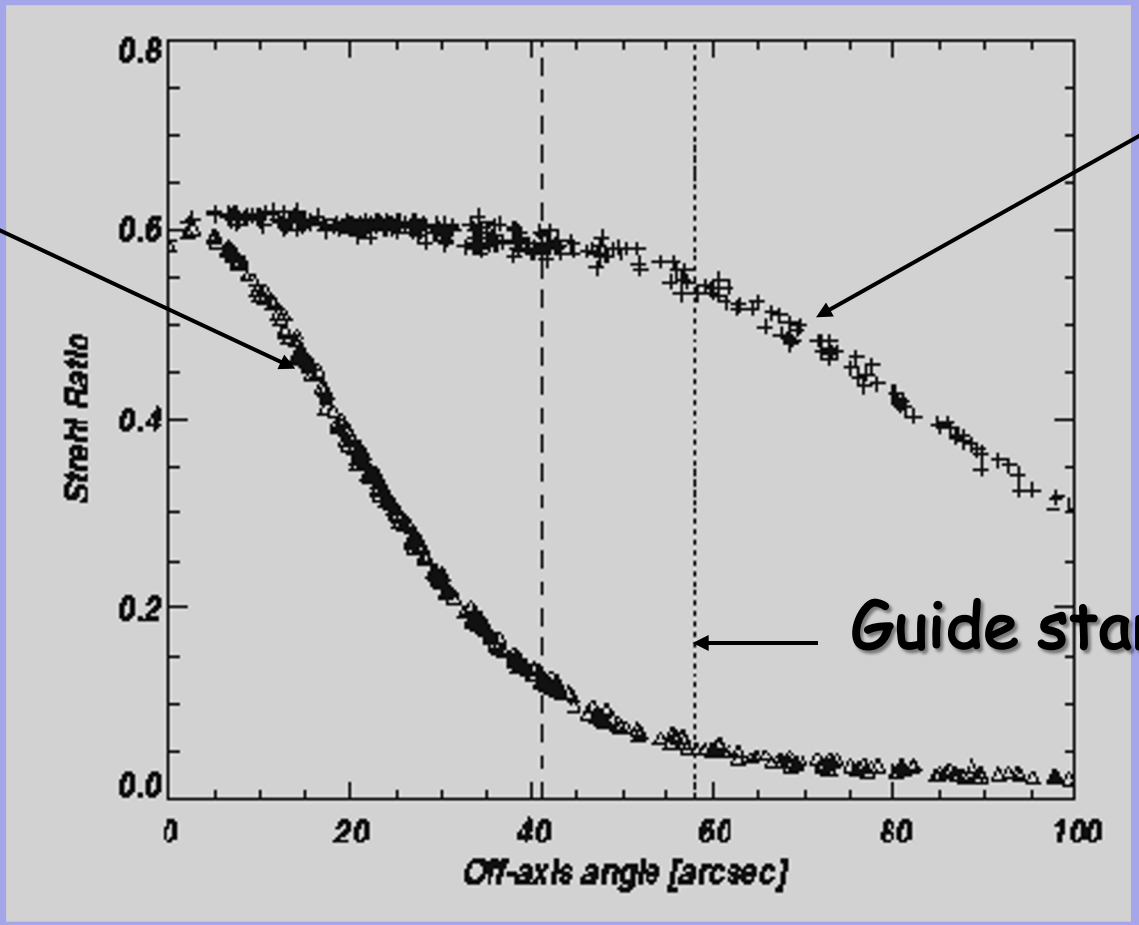

Laser Guide Stars

Substantial development programmes in sodium lasers, wavefront sensors, deformable mirrors, reconstructors and control systems

GEMS : LGS MCAO system on Gemini-S feeding GSAOI (Infrared AO Imager) or FLAMINGOS (IR Multi-object Spectrometer)

VLT AOF on UT4 is operating at Paranal feeding Hawk-I or MUSE

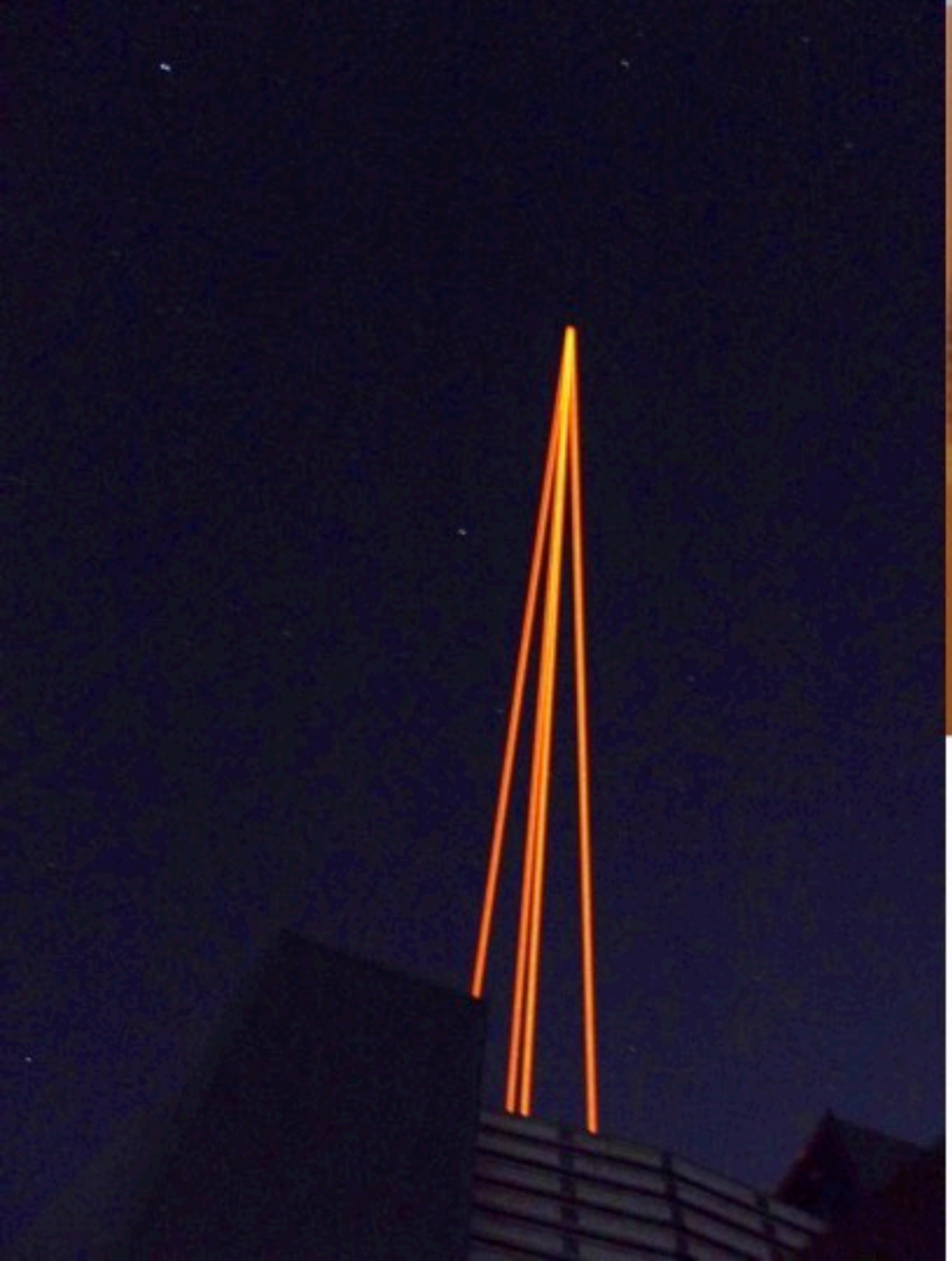

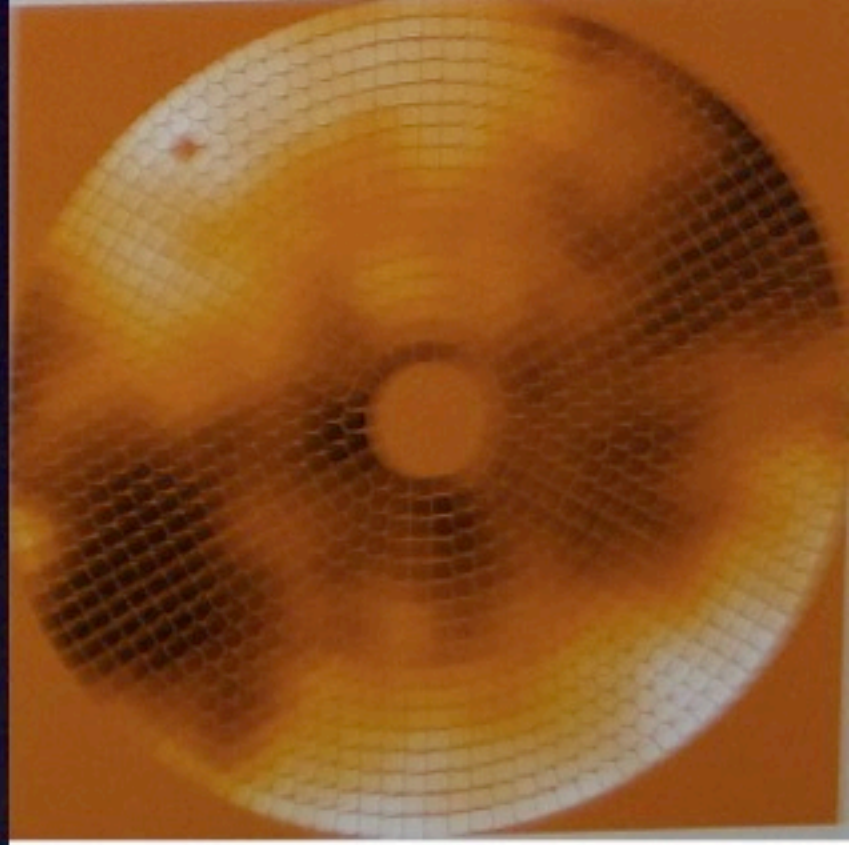

The LGS constellation produced by the adaptive Optics Facility at the UT4 telescope of the ESO VLT. Light from the LGS is used to estimate the wavefront distortions and corrections are applied to the deformable secondary mirror. The image above shows a snapshot of the phase corrections applied to the secondary.

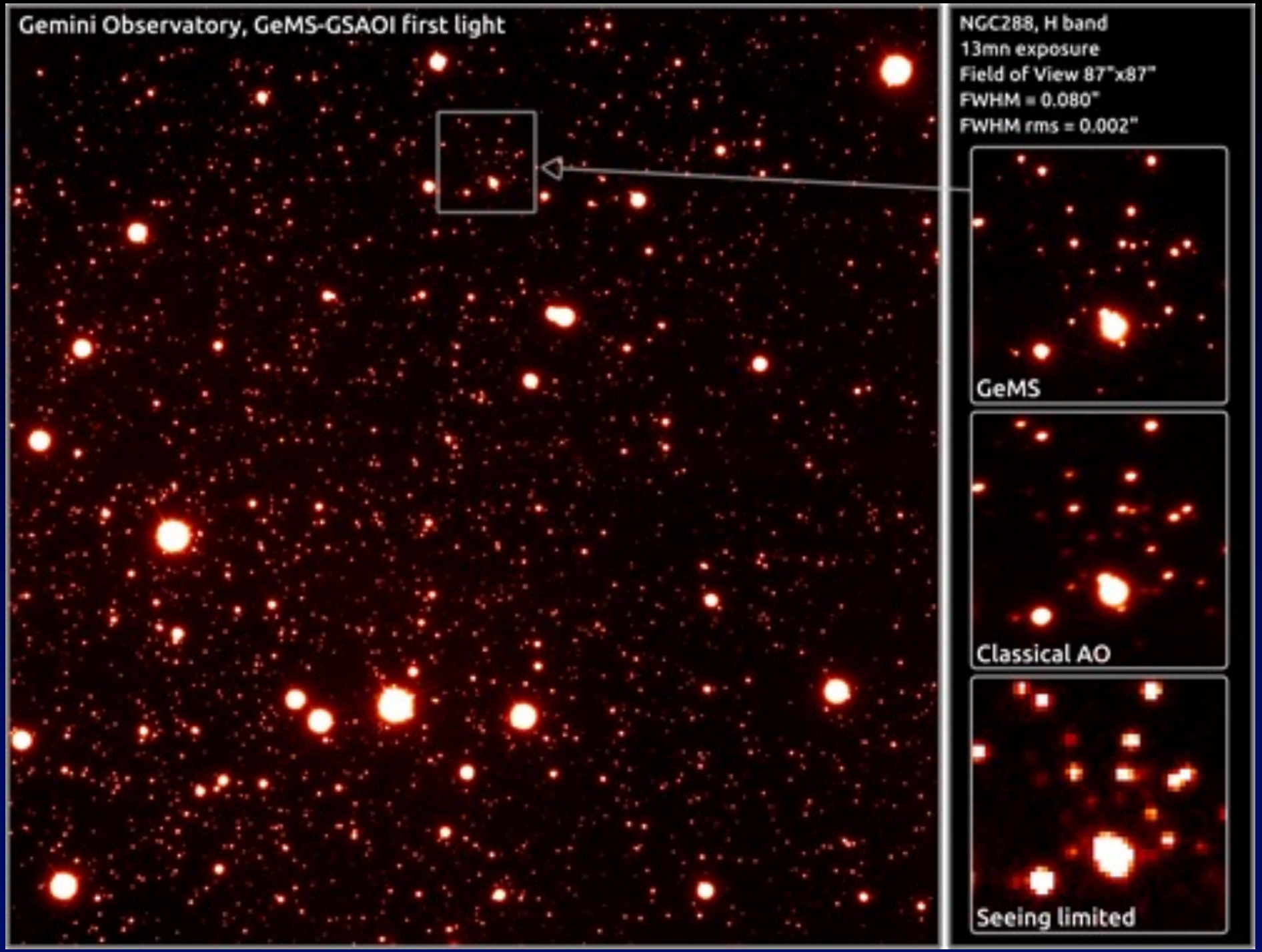
Gemini Observatory, GeMS-GSAOI first light
NGC288, H band
13mn exposure
Field of View 87"x87"
FWHM = 0.080"
FWHM rms = 0.002"
GeMS
Classical AO
Seeing limited

Different AO Flavours

Method		Corrected field of view
Laser Tomography AO	LTAO	10's of arc sec
Multi-Object AO	MOAO	N x 10's of arc sec
Multi-Conjugate AO	MCAO	≤ about 2 arc min
Ground Layer AO	GLAO	A few to 10 arc min

+ Extreme AO - aimed at very high Strehl on bright Natural Guide Stars – exoplanet searches

Challenges of AO

- Improved resolution, sharper images, but quite variable temporally and spatially, so calibration is tricky
- MCAO helps but is not widely available
- Uncorrected modes may still be significant, and often techniques such as Angular or Spectral Differential imaging are used to improve the subtraction of these effects (ADI or SDI).
- AO may be used with a coronagraph to suppress the light from the host star

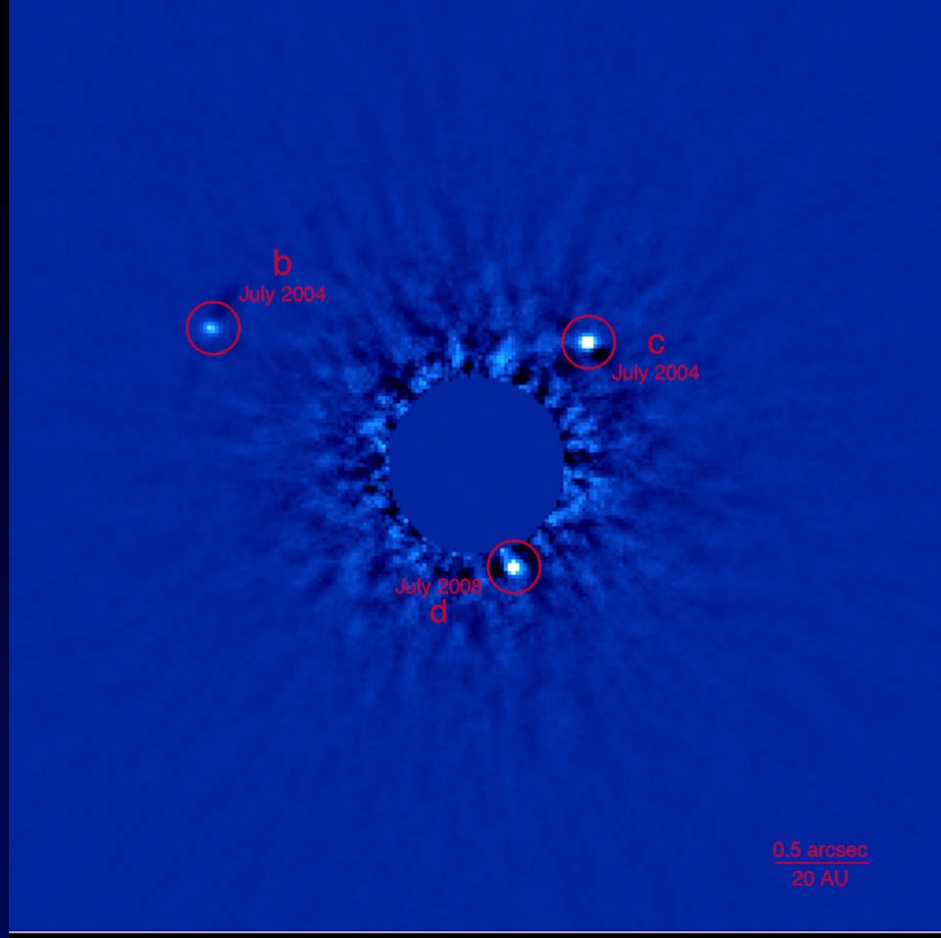

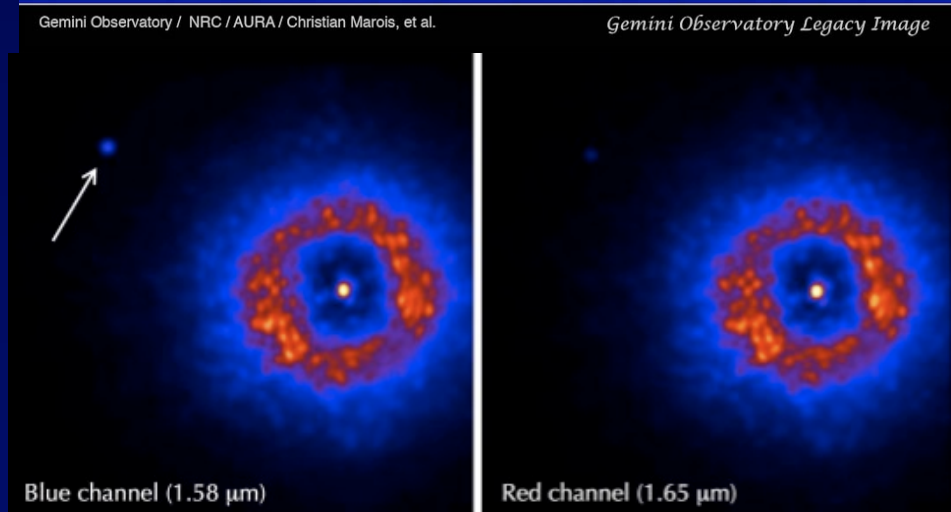

ADI (Angular Differential Imaging) + SDI (Spectral Differential Imaging)

- Residual image structure is partially due to aberrations in the telescope and instrument and uncorrected atmospheric structure
- In Angular Differential Imaging, a sequence of many exposures of the target is acquired using an altitude/azimuth telescope with the instrument rotator turned off (at the Cassegrain focus) to keep instrument and telescope optics aligned.
- This is a very stable configuration and ensures a high correlation of the sequence of PSF images, which would be smeared out if the rotator was used.
- The FOV rotates during the sequence, which has to be allowed for after subtraction of a reference image.
- Spectral Differential Imaging uses images obtained simultaneously on and off a spectral feature (e.g. the 1.6um methane absorption) where the aberrations are highly correlated because they are very close in wavelength
- Spectral deconvolution can be applied to spectrally dispersed Integral Field images (e.g. Thatte et al 2007). Here speckles and other aberrations increase in distance as a function of wavelength because of the increasing diffraction angle, but the separation of an object from its host star is at a fixed distance.

ADI illustrated with Gemini NIRI/Altair 1.6um observations (Lafreniere et al 2007)

(a) Original 30s image of the young star HD 691 after subtraction of an azimuthally symmetric median intensity profile.

(b and c) Corresponding residual image after ADI subtraction using the LOCI algorithm. . Display intensity ranges are 5 10^{-6} and 10^{-6} of stellar PSF peak for the top and bottom rows, respectively

(d) Median combination of 117 such residual images. Each panel is 10” on a side. The diffraction spikes from the secondary mirror support vanes and the central saturated region are masked. The faint point source visible in (d) at separation of 2.43” could not have been detected without ADI processing.

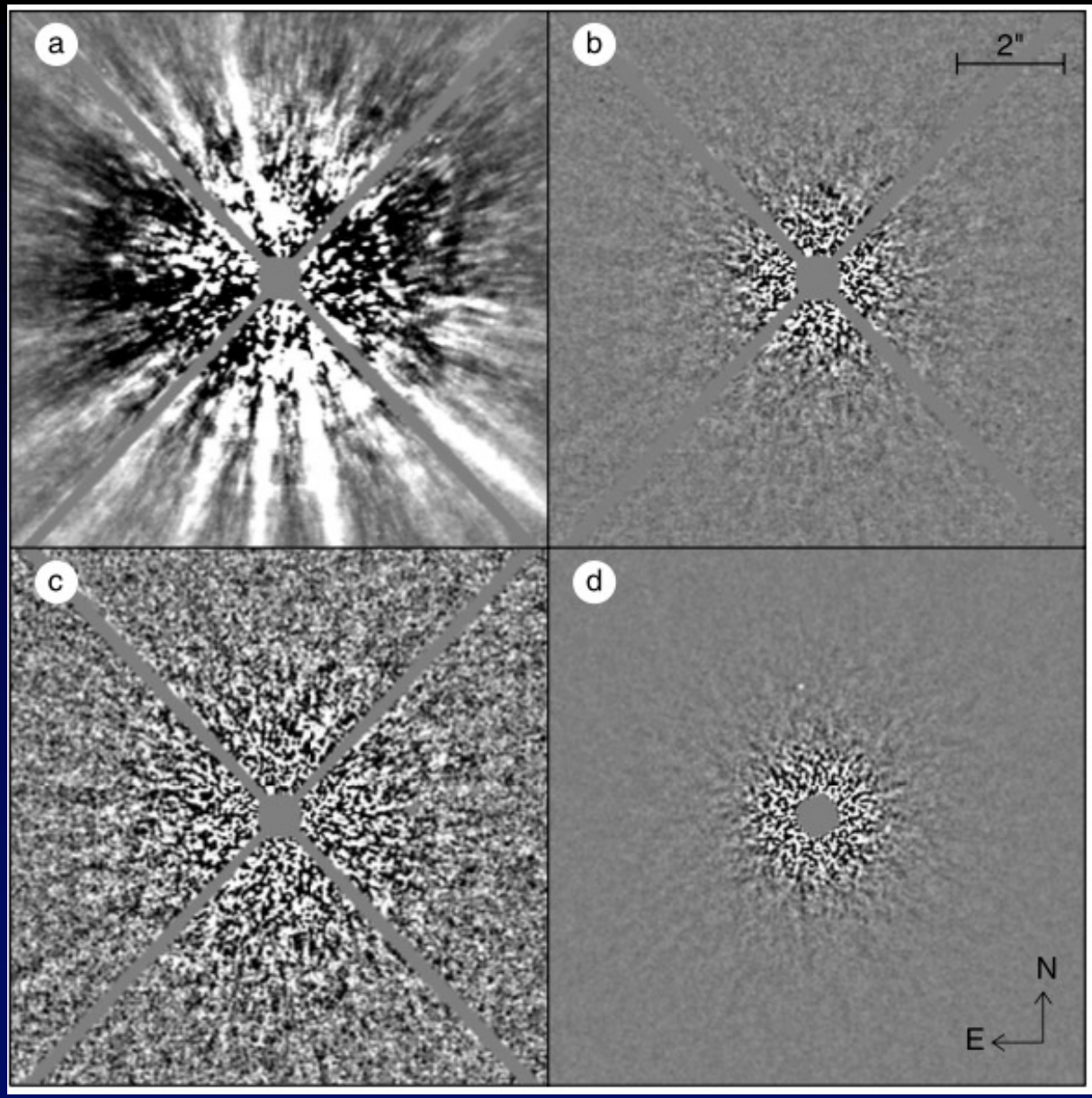

Spectral Deconvolution

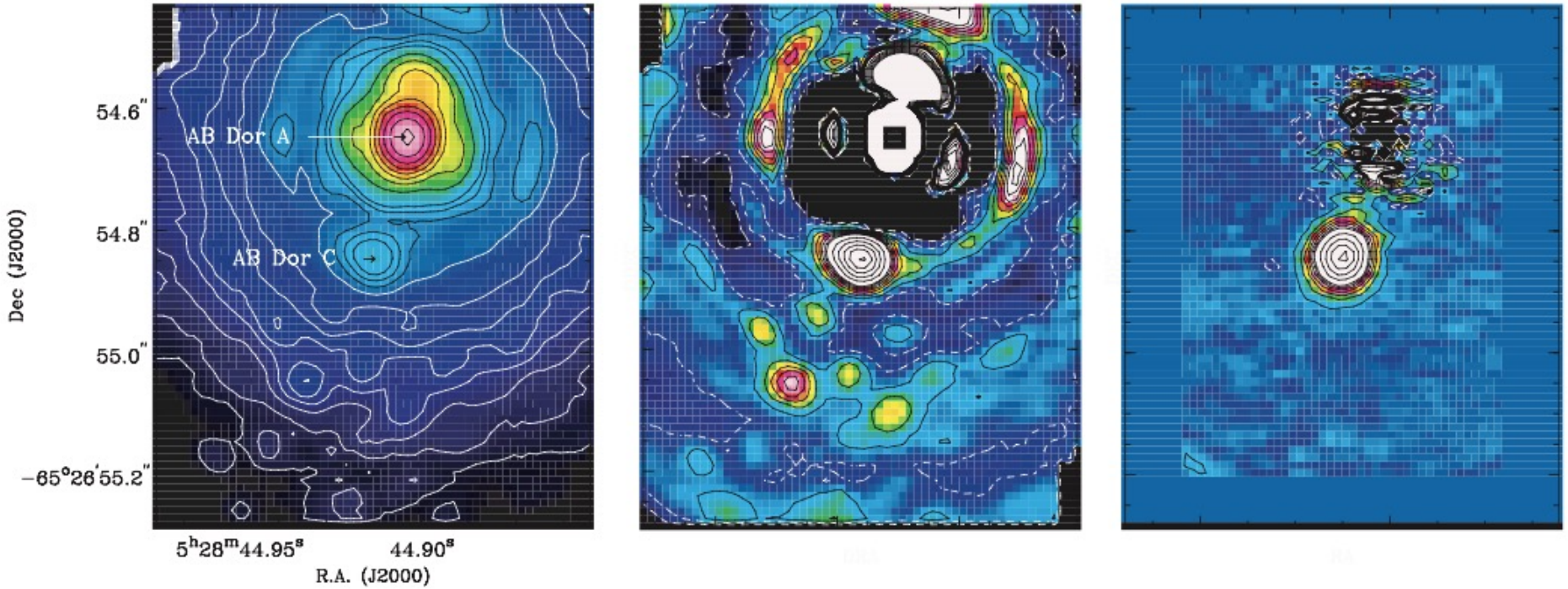

Figure 2. Illustration showing the efficacy of the SD technique at removing both PSF artefacts and super-speckles from the SINFONI IFS data cube for the AB Dor system. The left-hand frame shows one wavelength slice of the observed data cube at 2.2 μm. Note that the entire vertical extent of the image is only 0.9 arcsec. The colour table is logarithmic (minimum 10^1, maximum 10^4). The contours are logarithmic, from 0.9 to 2.3 in steps of 0.1, and from 2.3 to 4.0 in steps of 0.2. The middle frame shows the same data, but with a radial profile fitted and subtracted, so as to highlight the PSF imperfections. The super-speckles are easily confused with real sources in this narrow-band image. The colour table is now linear (minimum −10, maximum 25), with contours from −12.5 to 32.5 in steps of 5, and from 32.5 to 150 in steps of 20. The four-fold symmetry of the Airy pattern arises from the superposition of the diffraction spikes of the secondary support structure on the Airy rings. The right-hand frame shows the same wavelength slice of the data cube, after applying the SD technique iteratively. Colour table and contours are the same as for the middle frame. Super-speckles are completely absent at the lowest contour level of ±2.5, corresponding to a 1σ error of $\leqslant$1 unit.

Thatte et al 2007

For a review on AO and Astrophysics see e.g. Ric Davies & Markus Kisler, 2012, ARAA 50, 305

Sparse Aperture Mask Interferometry

Phase differences from a mask in NACO on the VLT data are shown in the lower left panel for two different pairs of holes (red and blue baselines, marked on the pupil image), exhibiting phase residuals of ~300 nm. In the lower right panel, the closure phase - the sum of three phases of three baselines formed by three separate holes (the triangle is given by black arrows in the pupil image) is given. Most of the phase noise from uncorrected seeing disappears, leaving a closure phase residual of 10 nm; an improvement by a factor of 30.

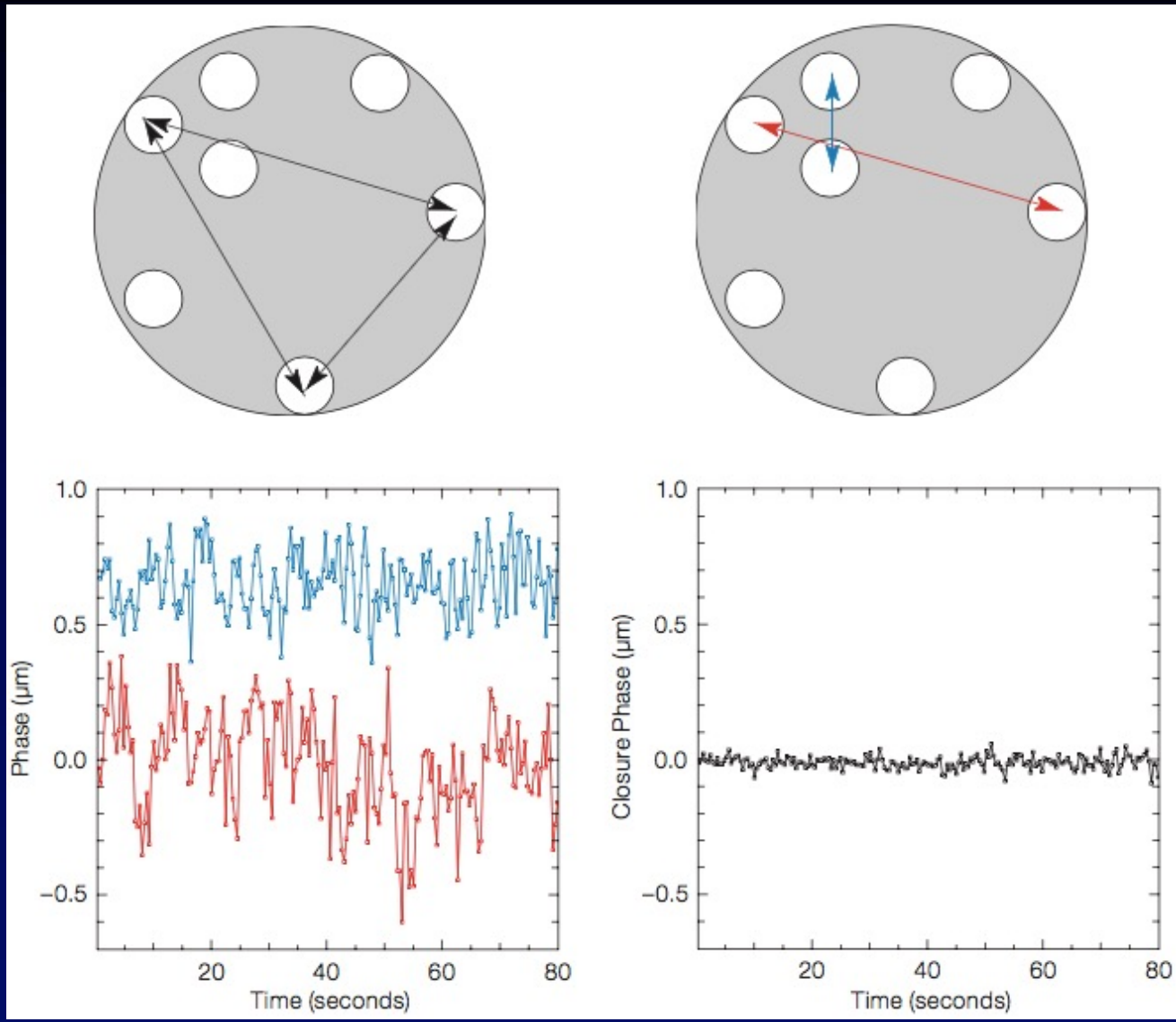

. (Lacour et al 2011)

Sparse Aperture Masking

SAM uses only a fraction of the light collected by the telescope, but provides enhanced stability and resolution, making it suitable for bright objects on large telescopes

This movie shows a sequence of 11 images of WR104, a late type dusty binary W-R star system obtained on the Keck 10-m telescope in the K-band. (P Tuthill et al 2008)

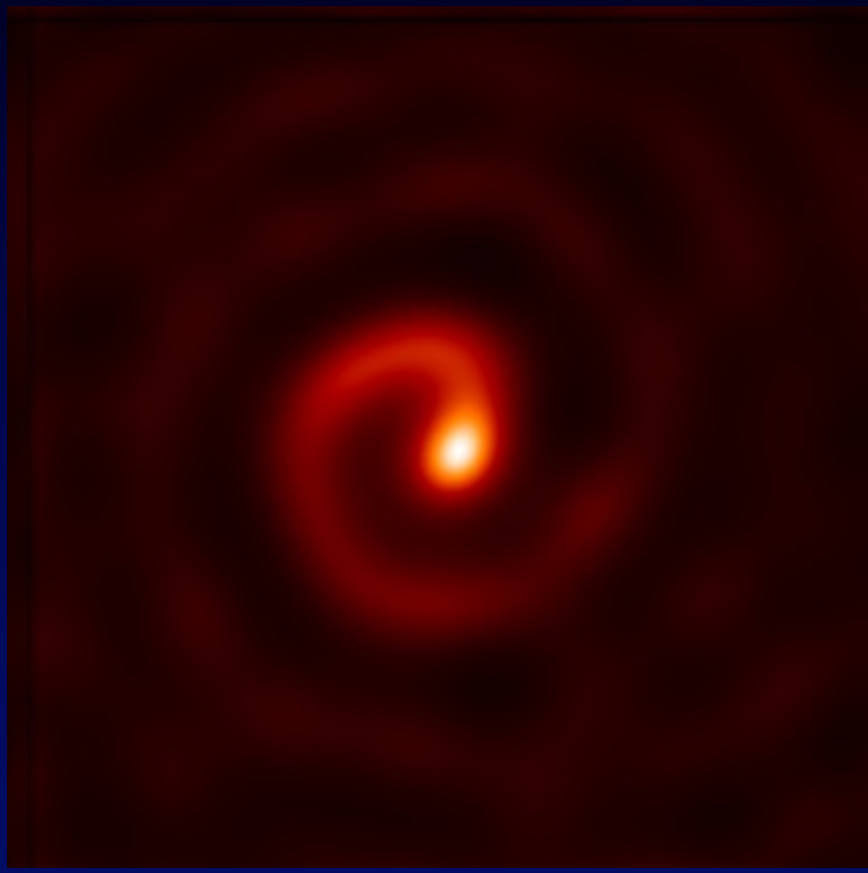

0.4 arcsec

Simulating a large telescope

- Arrange a discrete number of telescopes spread out over an area to cover the baselines of interest.
- 1 pair of telescopes → 1 baseline sensitive to a particular angular scale
- N telescopes → number of samples = $N(N\text{-}1)/2$
- As the Earth rotates the projected separation of the telescopes changes
- Sir Martin Ryle, (Cambridge) was awarded the 1974 Nobel Prize in Physics for developing Aperture Synthesis for radio astronomy

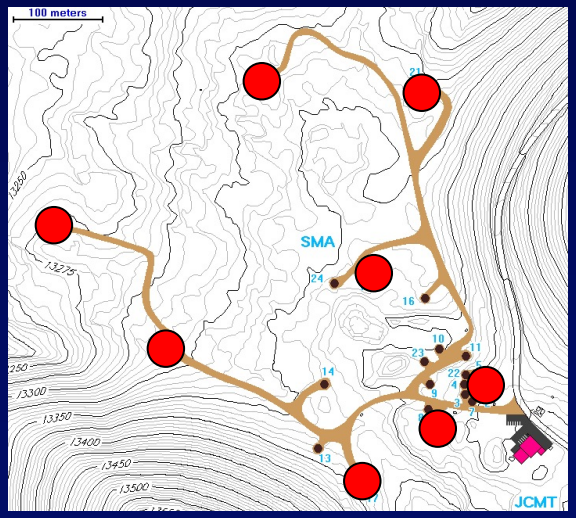

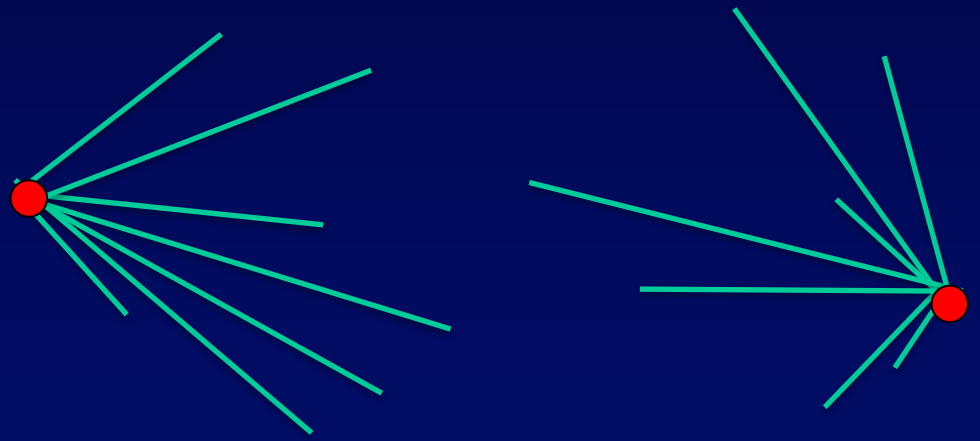

Interferometer Geometric Delay

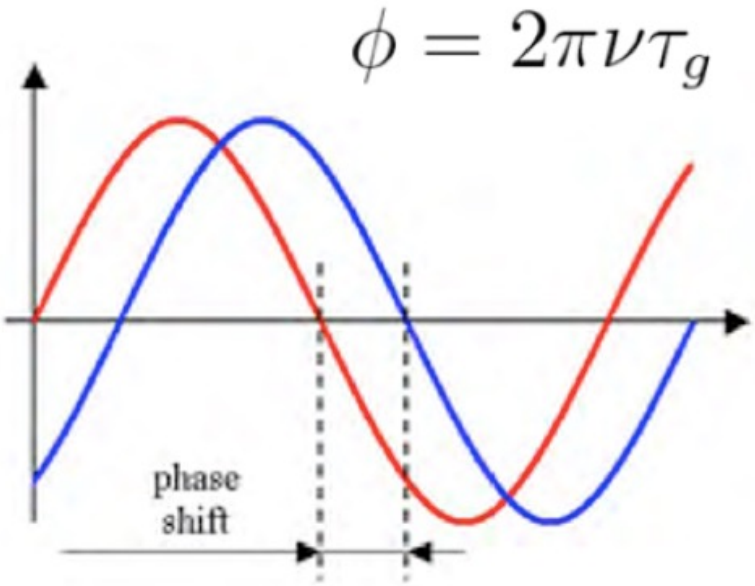

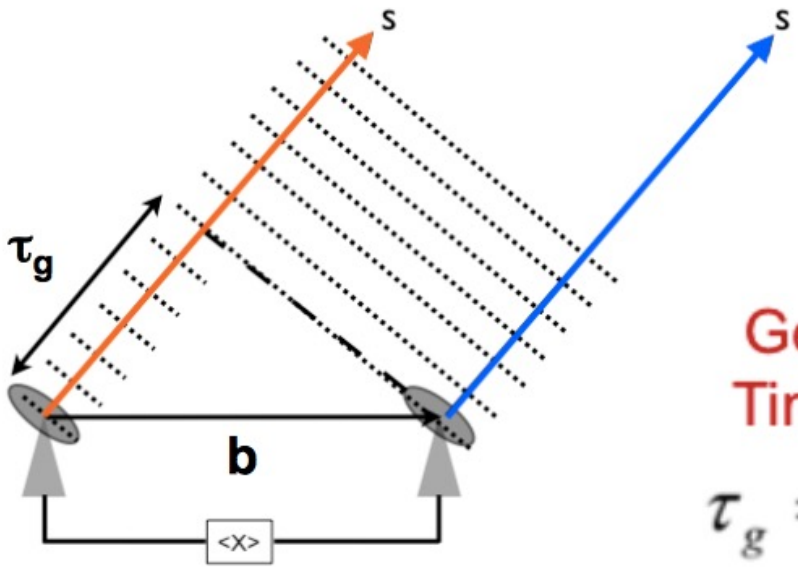

Geometric
Time Delay

$$\tau_g = \mathbf{b} \cdot \mathbf{s} / c$$

Because the telescopes are at different positions, the signal from an astronomical source arrives at different times. The geometric delay that arises from the physical separation of the telescopes or antennas has to be accounted for. This delay changes constantly as the Earth rotates.

Interferometry

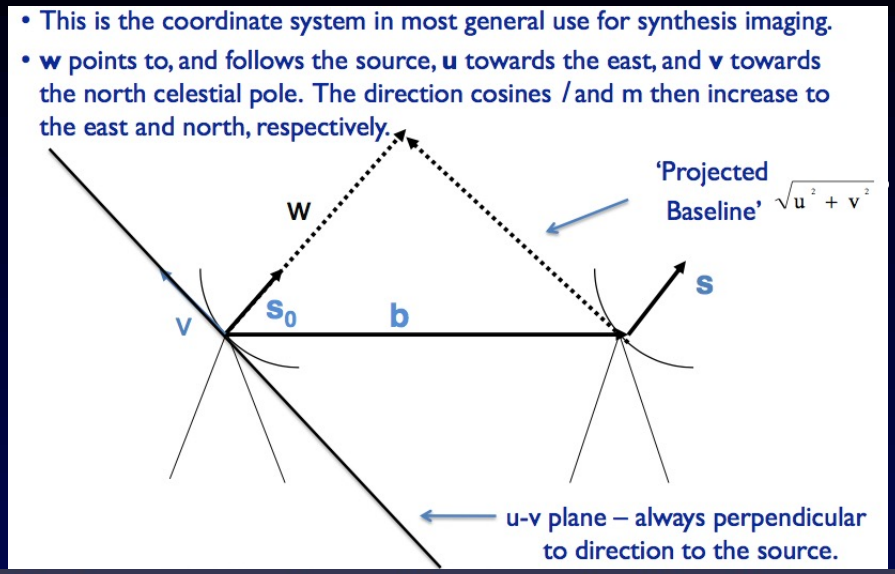

- Separated telescopes (antennas) generate fringes at spatial frequencies where the signal from an object is in phase.
- Increasing the number of telescopes increases the number of baselines, which increases the spatial frequencies sampled partial sampling leads to a complex psf

Telescope locations

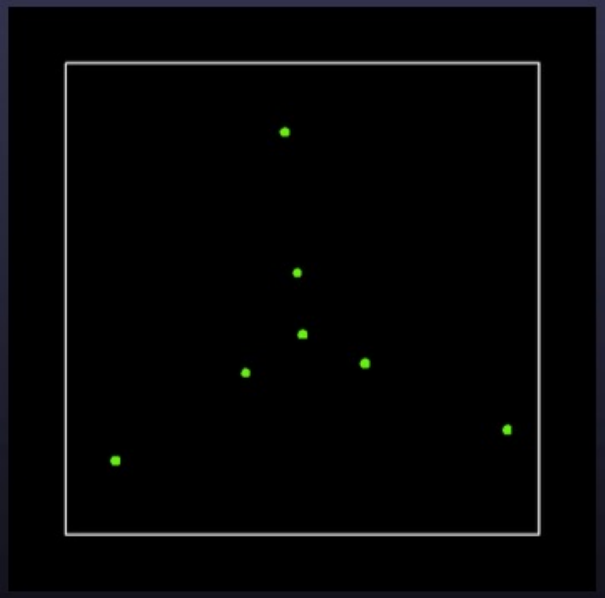

instantaneous *uv* coverage

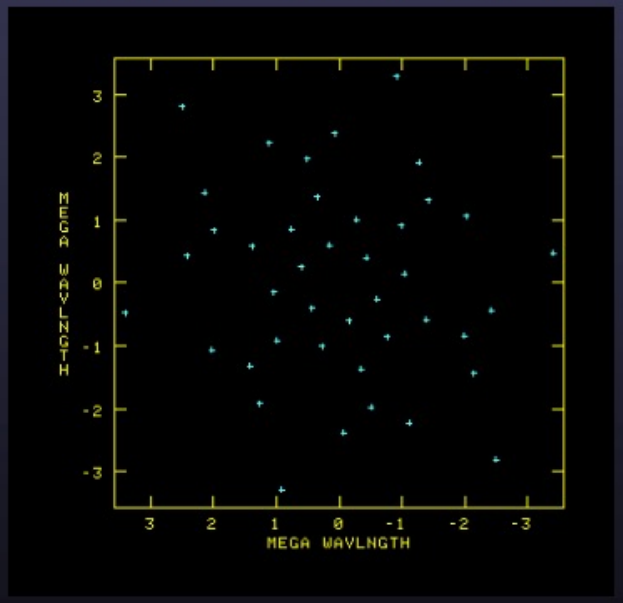

PSF

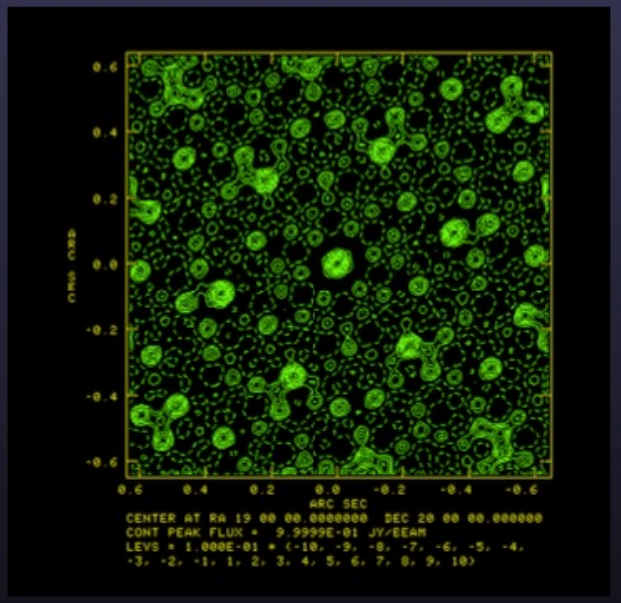

N(N-1)/2 baselines

8 Antennas

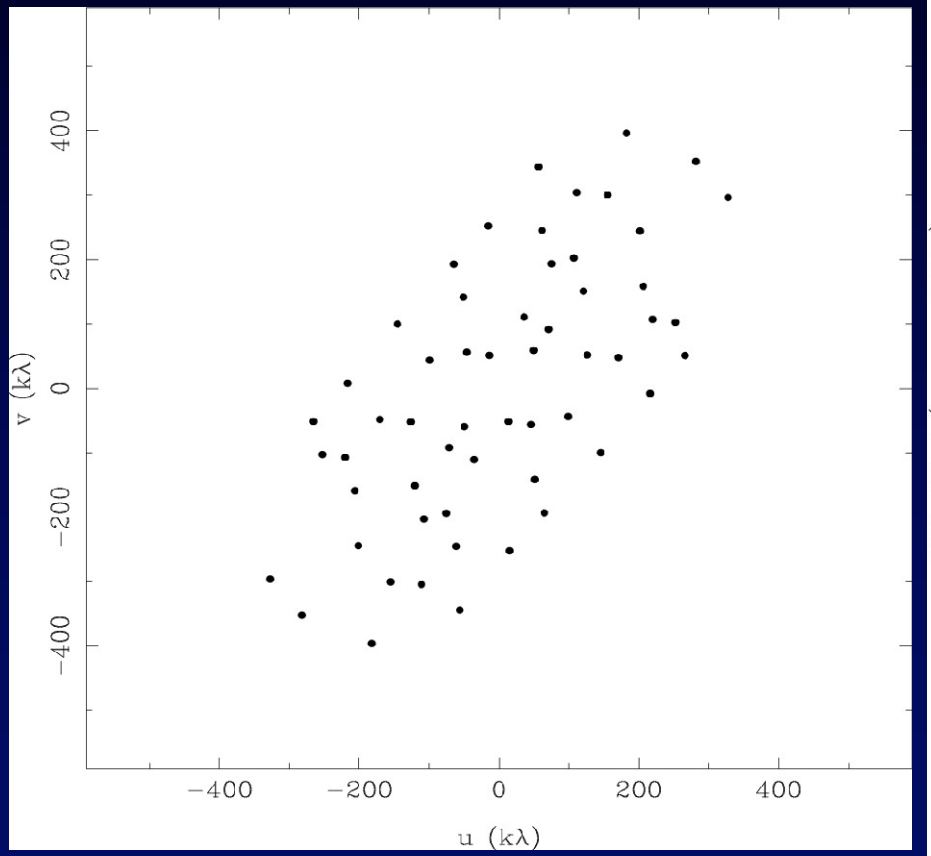

2-D antenna separations

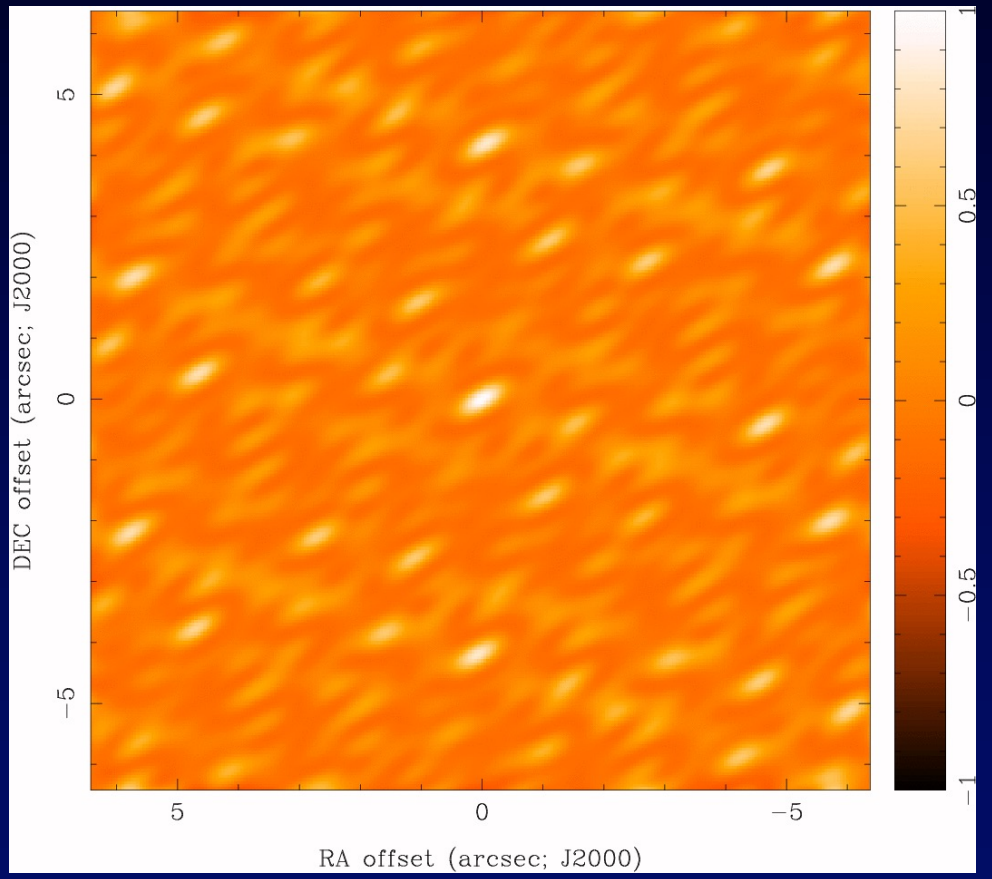

Corresponding image delivered

Effects of Earth's Rotation

8 Antennas x 480 Samples

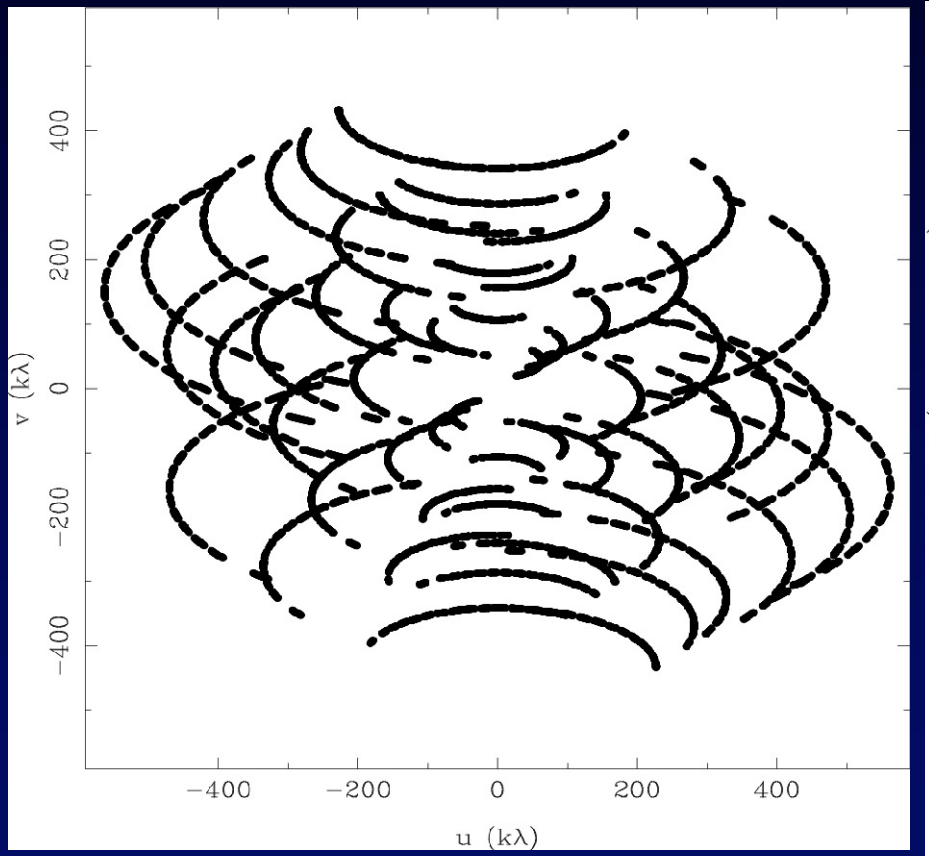

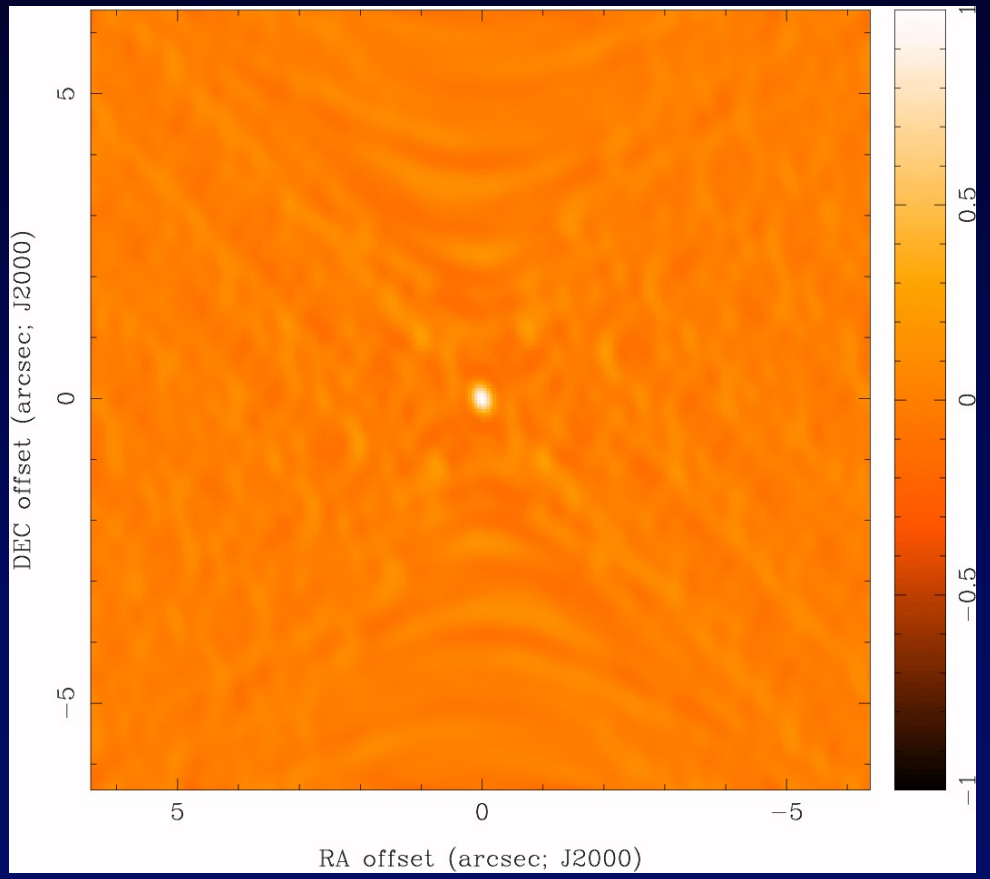

Increasing the number of baselines sharpens and cleans up the PSF

Top – 3 antennas on each arm of the VLA Y configuration

Middle – 8 antennas on each arm

Bottom - Earth rotation synthesis: As the object moves across the sky, the projected separation of the telescopes changes producing tracks of sampled baselines in the u-v plane (the plane normal to the line of sight to the object, improving sampling and thus the PSF

(Images from C Chandler)

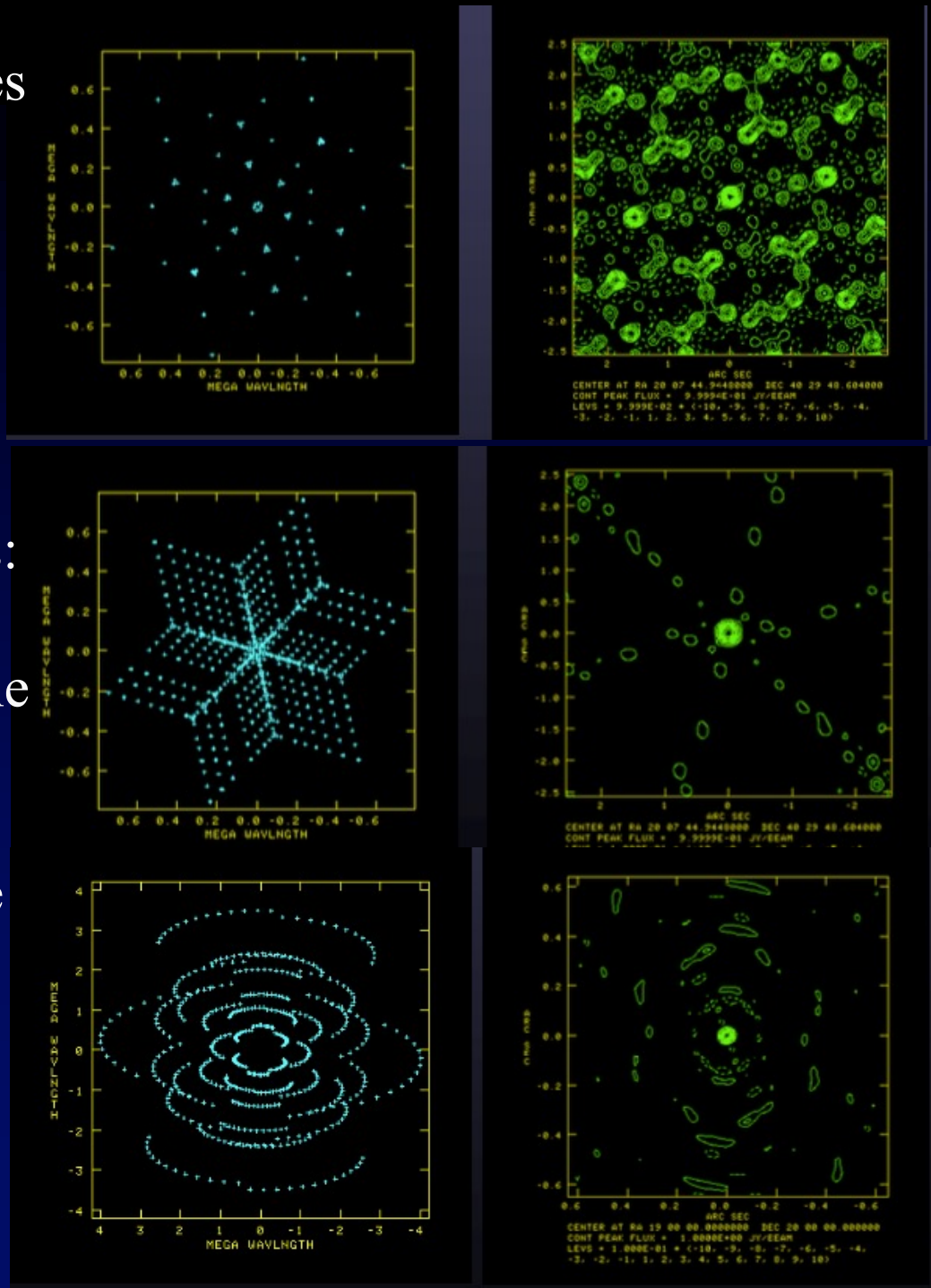

Images from Interferometry

- The signals from the antennas are multiplied together, or correlated, to give fringe amplitudes, which have a cos(ϕ) dependence
- The maximum resolution that can be obtained is given by the maximum baseline, while the maximum scale that is sampled is given by the minimum baseline. Interferometers rarely capture the total flux from an object, and so measurements may need to be complemented by measurements by a single aperture telescope or a more compact configuration (e.g. ALMA has 50 12-m antenna on baseline sup to 15km, togther with a compact array of 7-m antennas with baselines from 9 to 30 m
- Note that because of the cos(ϕ) dependence of the interferometer signal, rather than the sinc function of a single antenna, the resolution goes as $\lambda/2b$ rather than λ/D – so masks deployed on a single aperture telescope can increase the resolution.

Optical/IR interferometry

Separated telescopes allow longer baselines (~100m) to give milli-arcsec resolution at near-IR wavelengths, but with a small number of telescopes.

Interferometry at short wavelengths is restricted to ~6 telescopes because of the need to split the light in the correlation process

The VLTI offers 4 x 8-m UTs or 4 x 1.8m ATs. The telescopes need AO to fully use the apertures

Imaging is rather crude with 6 baselines and 4 different closure phases, but rotational synthesis means that good quality imaging is possible in the near-IR and soon in the mid-IR, when MATISSE is commissioned.

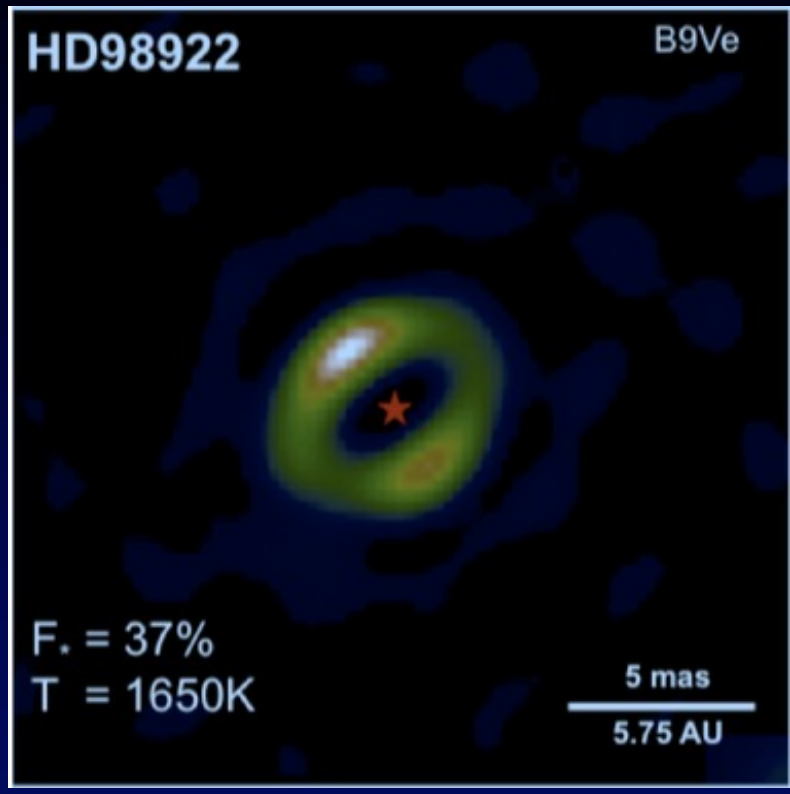

VLTI/PIONIER image reconstruction of the Be star HD98922 (Kluska et al 2013)

The VLTI

The light from the four 8-m VLT or four movable auxiliary telescopes can be combined to simulate a telescope with an aperture of 130m. This gives milliarcsec resolution

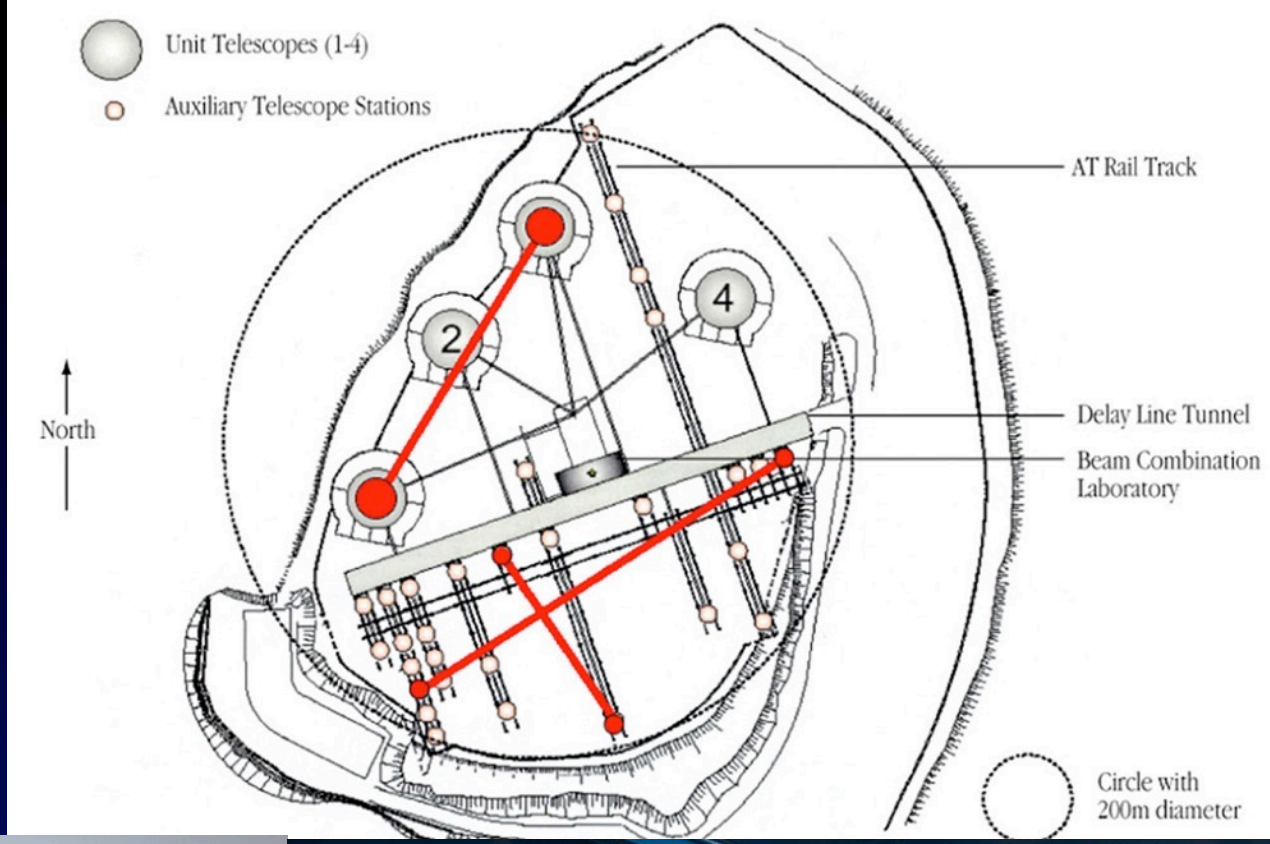

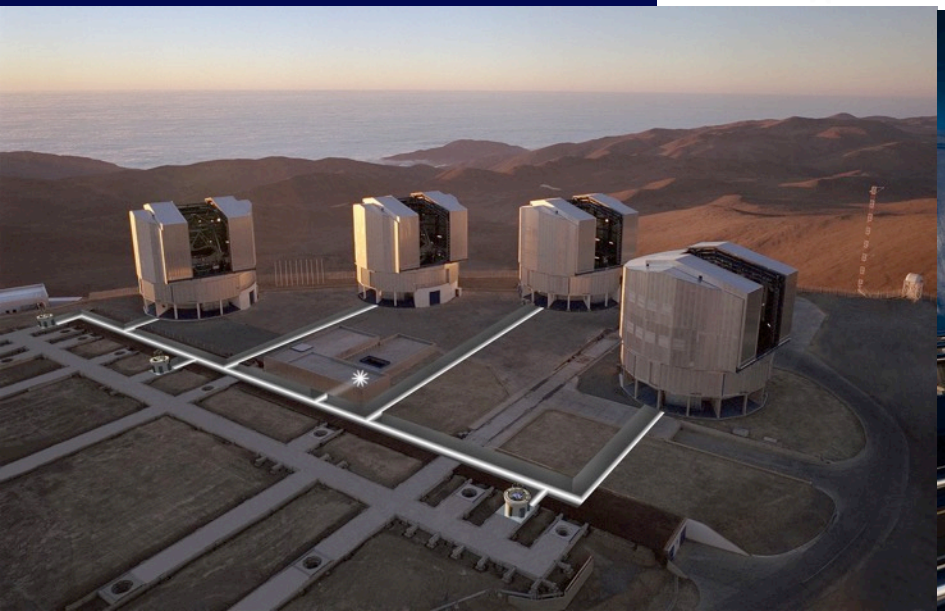

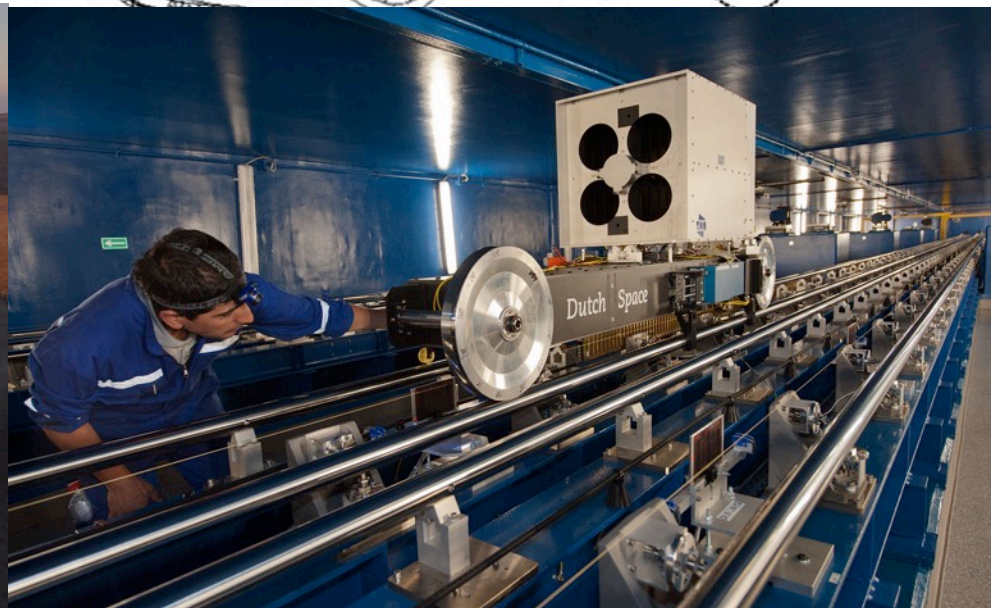

A new VLTI instrument, Gravity was commissioned in 2017. One of its prime targets is the measurement of the position of star S2 in its orbit and closest approach to the Black Hole.

It combines the infrared light from all four 8-m telescopes (or the four 1.8m auxiliary telescopes) to make precise measurements of the stars in the Galactic Centre and to investigate the origin of IR flares in Sgr A*. It requires very high precision control of hundreds of optical elements and compensation for vibrations

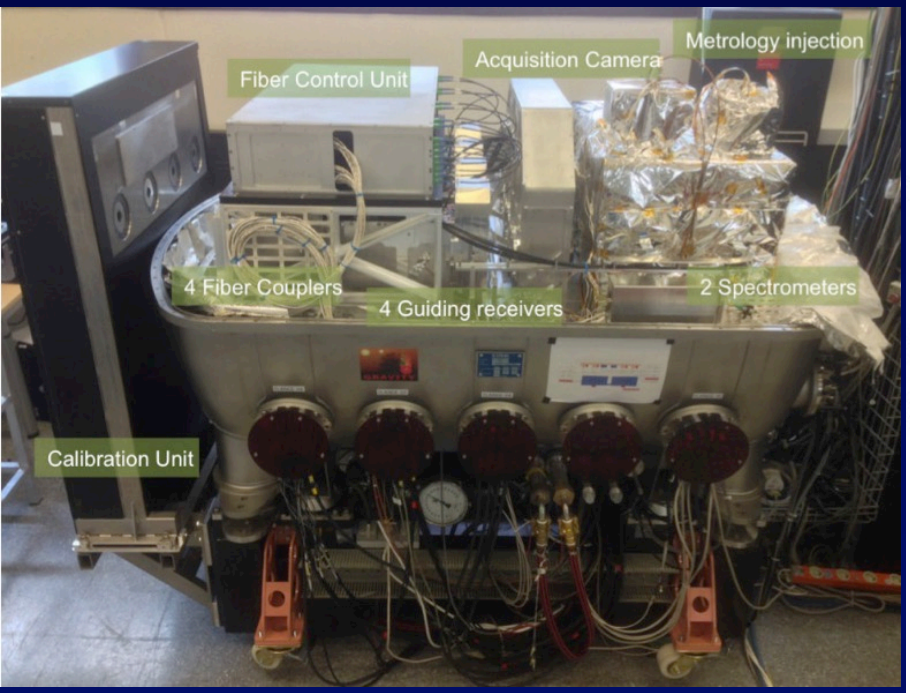

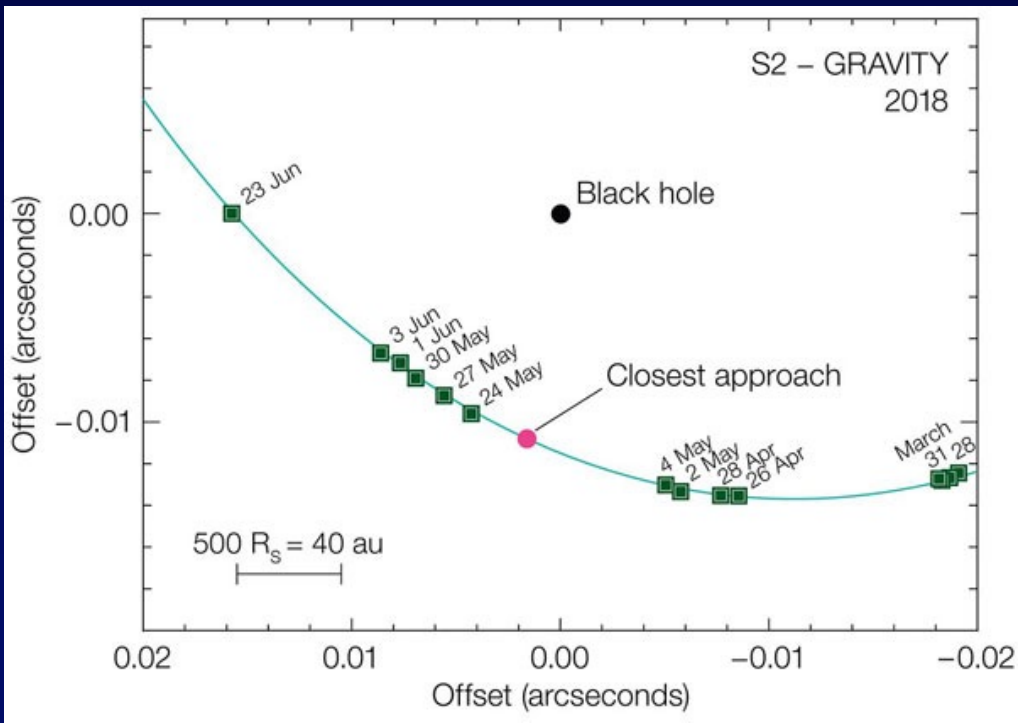

GRAVITY

GRAVITY has precisely measured the orbital position of star S2 as it moves through the Black Hole's gravitational potential, testing gravitational redshift and orbital precession in the strong gravity regime. The opportunity will not arise again until 2034

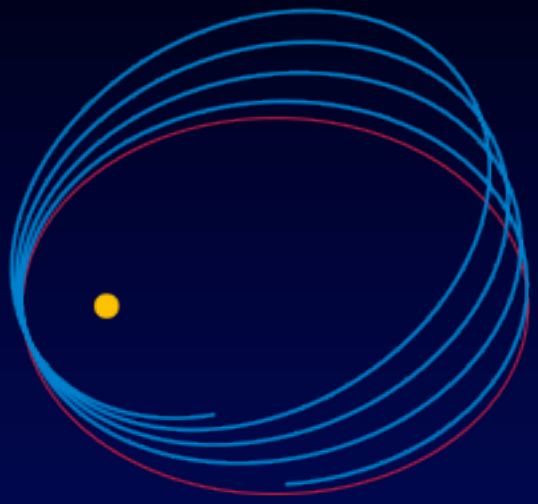

It has also located the position of theIR flares – The results indicate that they arise in an accretion disk around the Black Hole rather than in a jet of material ejected from the circumnuclear disk.

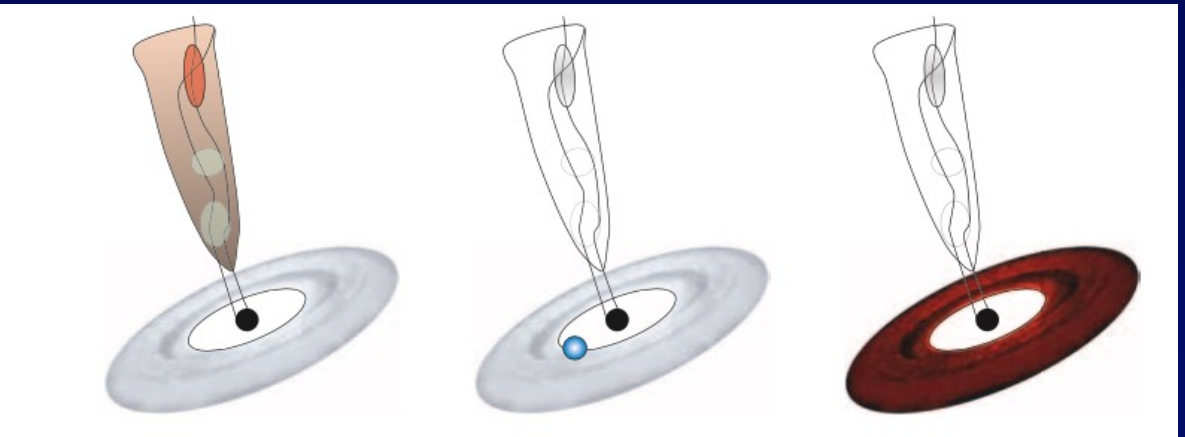

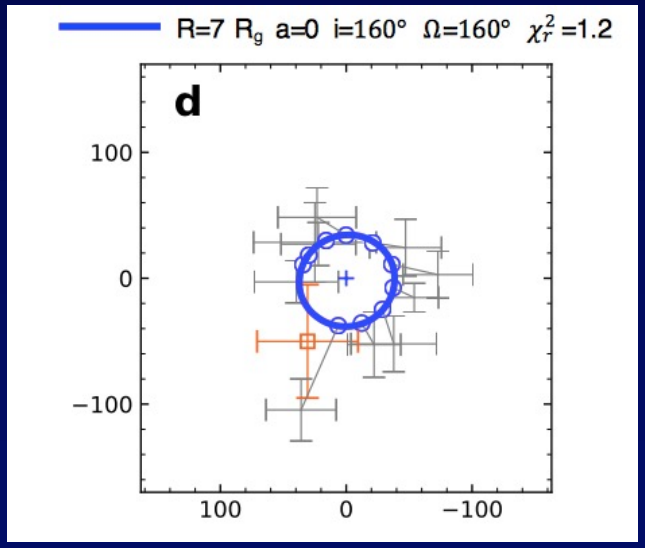

R Abuter et al 2018

Gravity team (MPE) Eisenhauer et al

GRAVITY's Firsts

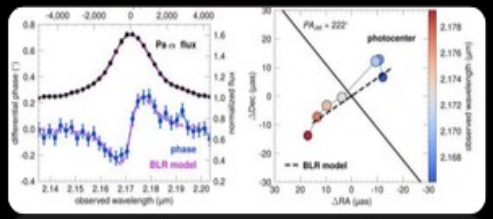

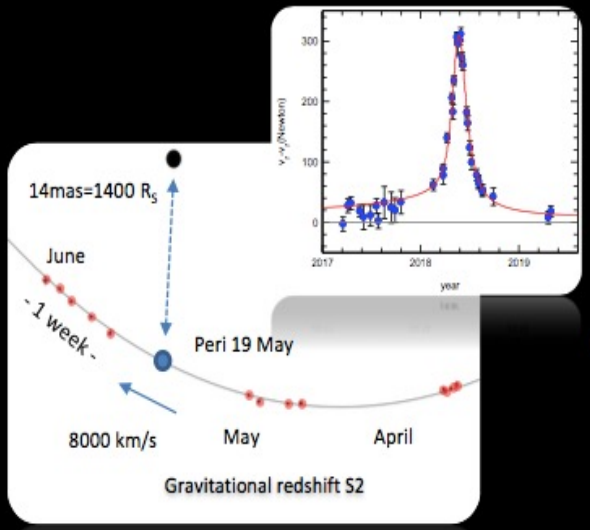

High resolution spectroscopy

19+ mag limiting magnitude & polarimetry

<50 µas imaging astrometry

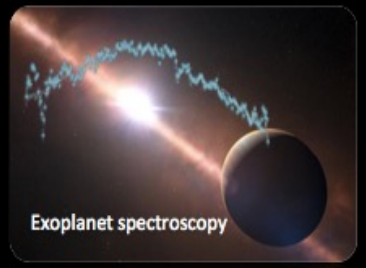

Micro-arcsec spectral differential astrometry

2 x 4 milli-arcsec resolution imaging

ALMA : Atacama Large Millimetre/sub-millimetre Array

66 Antennas on the Chajnantor plane at 5000-m in the Chilean Atacama desert operating between 0.3 – 3mm.
The antennas can be arranged in a variety of configurations with baselines from 500m to 15km

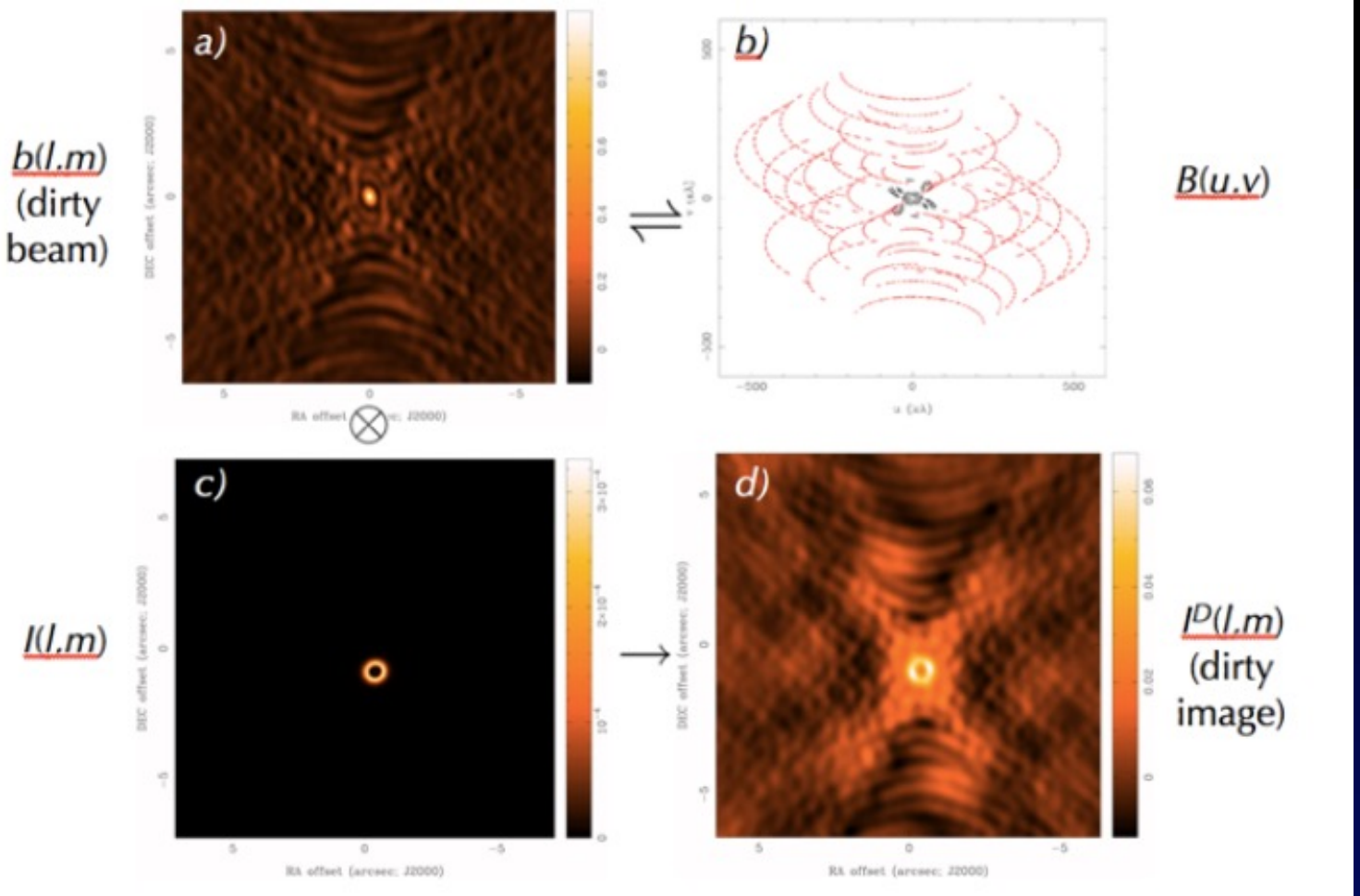

Figure 3.5: Imaging concepts. *Panel a (upper left)*: Example of a dirty beam, $b(l, m)$. *Panel b (upper right)*: The related ensemble of discrete points sampled in the uv-plane, $B(u, v)$. The black points were obtained from a compact configuration while the red ones were obtained from an extended configuration. *Panel c (lower left)*: Example of a true sky distribution, $I(l, m)$. *Panel d (lower right)*: The dirty image $I^D(l, m)$ resulting from observing $I(l, m)$ over the baselines of $B(u, v)$, or equivalently the convolution of $I(l, m)$ by $b(l, m)$. The antenna power response, $\mathcal{A}(l, m)$, has been ignored in this illustration since it is much wider than the true sky brightness distribution. (Figure courtesy of D. Wilner.)

Chapter 3 of the ALMA Technical Handbook gives a good introduction to interferometry, with lots of details of configurations, correlation etc.

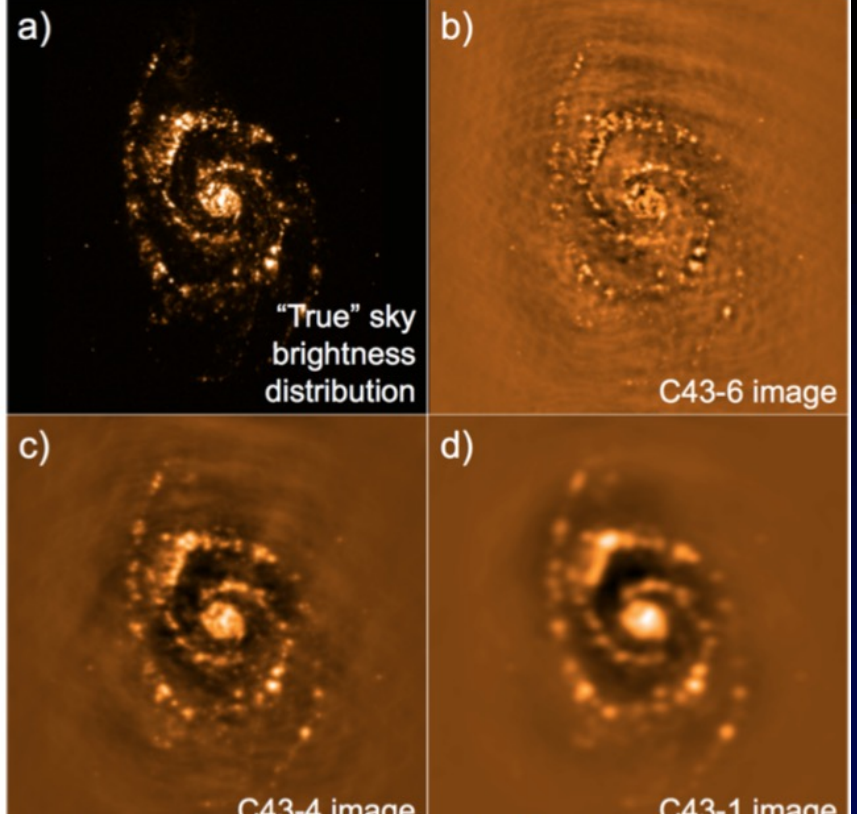

Figure 3.6: Examples of spatial filtering using the CASA task *simobserve* and actual ALMA configurations for Cycle 7. *Panel a (upper left)*: An optical image of the galaxy M51 used as a template for a true sky brightness distribution for the simulations. The frequency of the emission has been changed to 100 GHz, the image size has been scaled to $\sim 3' \times 3'$, and its declination has been changed to -40° to allow ALMA observations to be simulated. For the simulations, the galaxy was "observed" over a mosaic of 33 pointings, for ~10 hours in total. The resulting dirty images were CLEANed. *Panel b (upper right)*: The high-resolution image of the galaxy obtained when observed in the ALMA C43-6 configuration with maximum baseline of 2516.9 m, respectively. The resulting synthesized beam is $\sim 0.47''$ and the maximum recoverable scale is $\sim 4''$. *Panel c (lower left)*: Medium-resolution image of the galaxy when observed in the ALMA C43-4 configuration with maximum baseline of 783.5 m, respectively. The resulting synthesized beam is $\sim 1.3''$ and the maximum recoverable scale is $\sim 11''$. *Panel d (lower right)*: Low-resolution image of the galaxy when observed in ALMA configuration C43-1 with maximum baselines of 160.7 m, respectively. The resulting synthesized beam is $\sim 4.3''$ and the maximum recoverable scale is $\sim 28''$.

ALMA Interferometer Configurations

Configuration	7-m	C43-1	C43-2	C43-3	C43-4	C43-5
Minimum baseline (m)	8.7	14.6	14.6	14.6	14.6	14.6
5th percentile or L05 (m)	9.1	21.4	27.0	37.6	54.1	90.9
80th percentile or L80 (m)	30.7	107.1	143.8	235.4	369.2	623.8
Maximum baseline (m)	45.0	160.7	313.7	500.2	783.5	1397.9
Configuration	C43-6	C43-7	C43-8	C43-9	C43-10	
Minimum baseline (m)	14.6	64.0	110.4	367.6	244.0	
5th percentile or L05 (m)	148.6	235.2	427.3	746.9	1228.1	
80th percentile or L80 (m)	1172.5	1673.1	3527.3	6482.6	8685.9	
Maximum baseline (m)	2516.9	3637.8	8547.7	13894.2	16194.0	

Table 7.2: Basic parameters of the 7-m Array configuration and the ten 12-m Array configurations offered during Cycle 7. The baselines are projected for a transiting source (HA $= \pm$ 1h) at a declination of $-23°$. Note that C43-8 and C43-10 will not be available for Bands 8-10.

The ALMA 12-m dishes only occupy 50 of the available 192 antenna pads, and can be arranged with maximum baselines from 150m to 15km.

In practice a limited number of configurations is used and they are scheduled according to the seasonal constraints (high frequency, long baseline observations are not possible in the worst weather) and RA requirements of the science programme.

The highest resolution is obtained with Very Long Baseline Interferometry – transcontinental baselines, where correlation is does off-site on accurately time-stamped data from large dishes.

	Band	3	4	5	6	7	8	9	10
	Frequency (GHz)	100	150	185	230	345	460	650	870
Configuration									
7-m	θ_{res} (arcsec)	12.5	8.35	6.77	5.45	3.63	2.72	1.93	1.44
	θ_{MRS} (arcsec)	66.7	44.5	36.1	29.0	19.3	14.5	10.3	7.67
C43-1	θ_{res} (arcsec)	3.38	2.25	1.83	1.47	0.98	0.735	0.52	0.389
	θ_{MRS} (arcsec)	28.5	19.0	15.4	12.4	8.25	6.19	4.38	3.27
C43-2	θ_{res} (arcsec)	2.3	1.53	1.24	0.999	0.666	0.499	0.353	0.264
	θ_{MRS} (arcsec)	22.6	15.0	12.2	9.81	6.54	4.9	3.47	2.59
C43-3	θ_{res} (arcsec)	1.42	0.943	0.765	0.615	0.41	0.308	0.218	0.163
	θ_{MRS} (arcsec)	16.2	10.8	8.73	7.02	4.68	3.51	2.48	1.86
C43-4	θ_{res} (arcsec)	0.918	0.612	0.496	0.399	0.266	0.2	0.141	0.106
	θ_{MRS} (arcsec)	11.2	7.5	6.08	4.89	3.26	2.44	1.73	1.29
C43-5	θ_{res} (arcsec)	0.545	0.363	0.295	0.237	0.158	0.118	0.0838	0.0626
	θ_{MRS} (arcsec)	6.7	4.47	3.62	2.91	1.94	1.46	1.03	0.77
C43-6	θ_{res} (arcsec)	0.306	0.204	0.165	0.133	0.0887	0.0665	0.0471	0.0352
	θ_{MRS} (arcsec)	4.11	2.74	2.22	1.78	1.19	0.892	0.632	0.472
C43-7	θ_{res} (arcsec)	0.211	0.141	0.114	0.0917	0.0612	0.0459	0.0325	0.0243
	θ_{MRS} (arcsec)	2.58	1.72	1.4	1.12	0.749	0.562	0.398	0.297
C43-8	θ_{res} (arcsec)	0.096	0.064	0.0519	0.0417	0.0278	-	-	-
	θ_{MRS} (arcsec)	1.42	0.947	0.768	0.618	0.412	-	-	-
C43-9	θ_{res} (arcsec)	0.057	0.038	0.0308	0.0248	0.0165	-	-	-
	θ_{MRS} (arcsec)	0.814	0.543	0.44	0.354	0.236	-	-	-
C43-10	θ_{res} (arcsec)	0.042	0.028	0.0227	0.0183	0.0122	-	-	-
	θ_{MRS} (arcsec)	0.496	0.331	0.268	0.216	0.144	-	-	-

Table 7.1: Resolution (θ_{res}) and maximum recoverable scale (θ_{MRS}) for the 7-m Array and 12-m Array configurations available during Cycle 7 as a function of a representative frequency in a band. The value of θ_{MRS} is computed using the 5$^{\text{th}}$ percentile baseline (L05) from Table 7.2 and Equation 7.7. The value of θ_{res} is the mean

The Event Horizon Telescope Intercontinental Baselines

Giving resolutions of 15 micro-arcsec or about 1.5 times the Event Horizon radius
Data streams from the individual telescopes are time stamped using atomic clocks and then correlated together and analysed

ALMA and the EHT

- Very Long Baseline Interferometry requires careful co-ordination between the observatories, observing simultaneously to simulate an Earth-sized telescope.
- The first run observing the Galactic Centre and M87 was in April 2017
- ALMA used 45 co-phased 12-m diameter dishes equivalent to an 80-m diameter telescope
  - Because of the data rates, and the need to correlate raw datastreams, hard disks have to be flown from the South Pole, which only became possible in November 2017.

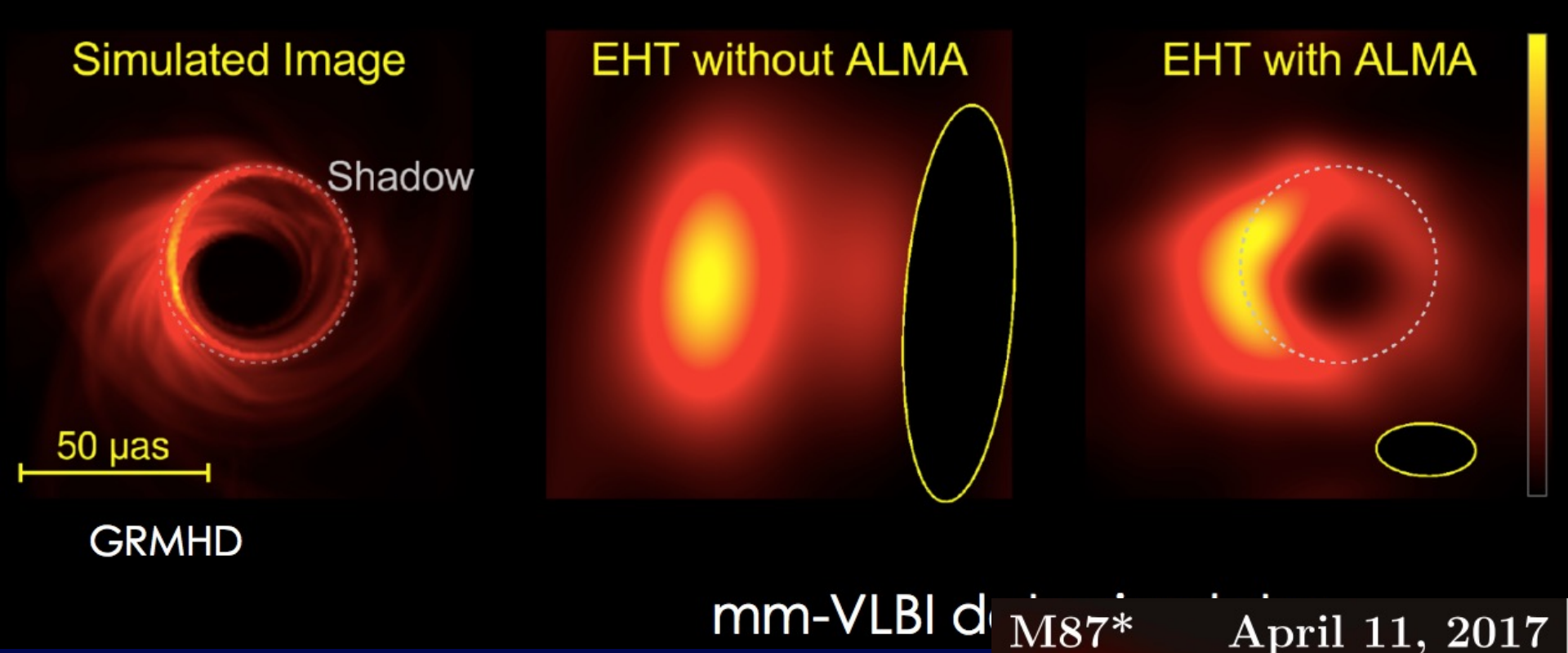

ALMA makes a big difference – largest collecting area and greatest sensitivity – essential for north-south coverage.

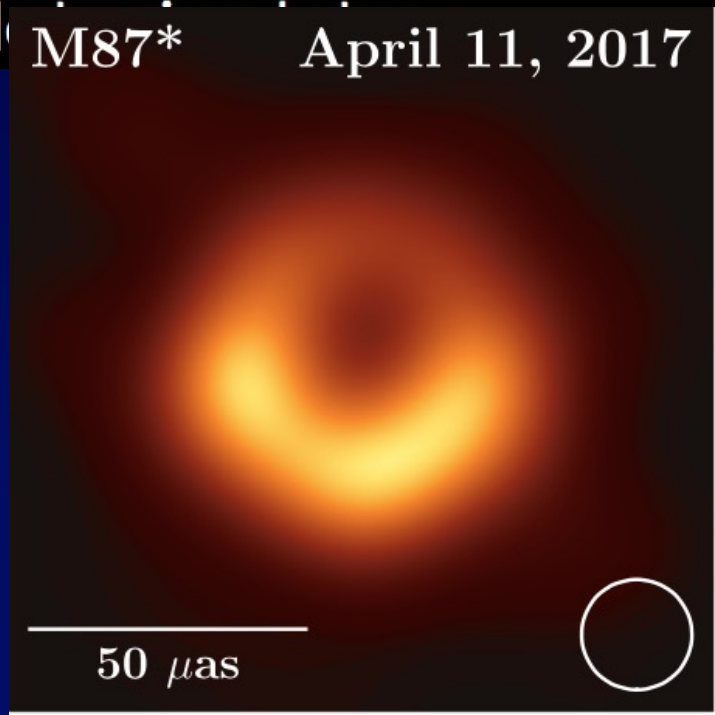

EHT

The combination of mm-wavelength observations and very long, transcontinental baseline gives the EHT the resolution needed to image the immediate vicinity of the Black Hole